Asynchronous Fractional Multi-Agent Deep Reinforcement Learning for Age-Minimal Mobile Edge Computing

Lyudong Jin, Ming Tang, *Member, IEEE*, Jiayu Pan, Meng Zhang, *Member, IEEE*, Hao Wang, *Member, IEEE*

arXiv:2409.16832v2 [cs.LG] 8 Oct 2024

***Abstract*—In the realm of emerging real-time networked applications like cyber-physical systems (CPS), the *Age of Information (AoI)* has merged as a pivotal metric for evaluating the timeliness. To meet the high computational demands, such as those in intelligent manufacturing within CPS, mobile edge computing (MEC) presents a promising solution for optimizing computing and reducing AoI. In this work, we study the timeliness of computational-intensive updates and explore jointly optimizing the task updating (when to generate a task) and offloading (where to process a task) policies to minimize AoI. Specifically, we consider edge load dynamics and formulate a task scheduling problem to minimize the expected time-average AoI. Solving this problem is challenging due to the fractional objective introduced by AoI and asynchronous decision-making of the semi-Markov game (SMG). To this end, we propose a fractional reinforcement learning (RL) framework. We first introduce a fractional single-agent RL framework and further propose a fractional multi-agent RL framework, including convergence analysis for both scenarios. To tackle the challenge of asynchronous decision-making in SMG, we further design an asynchronous model-free fractional multi-agent RL algorithm, where each mobile device can determine the task updating and offloading decisions without knowing the real-time system dynamics and decisions of other devices. Experimental results show that when compared with the best baseline algorithm, our proposed algorithms reduce the average AoI by up to 52.6%.**

***Index Terms*—Age of Information, mobile edge computing, Nash equilibrium, reinforcement learning, multi-agent reinforcement learning**

I. Introduction

A. Background and Motivations

Real-time embedded systems and mobile devices, including smartphones, IoT devices, and wireless sensors, have rapidly proliferated. This growth is driven by cyber-physical systems (CPS) applications including collaborative autonomous driving (e.g., [2]), smart power grid (e.g., [3]), and intelligent manufacturing (e.g., [4]). These applications generate a large amount of data and require intensive processing. This drives the needs for low latency, reliable, and private task processing. Mobile edge computing (MEC), also known as multi-access edge computing [5], addresses these needs by offloading computational tasks from end devices to nearby edge servers [6]. In this way, MEC reduces latency compared to cloud computing and provide larger computational capacity than that of mobile computing.

Additionally, timely information updates are crucial in CPS. These updates involve refreshing computed results such as traffic predictions, object detection outcomes, and system optimization solutions. They are vital for emerging CPS applications (e.g., [7]–[9]), including IoT-based ambient intelligence, autonomous driving, and industrial metaverse applications and so on. For instance, critical applications (e.g., [10], [11]), such as high-resolution video crowd-sourcing and real-time collision warning, rely heavily on timely data processing and updates. Local computing often struggles to meet these stringent timeliness requirements, compromising system performance and safety. This need for data freshness leads to the development of a new metric *Age of Information (AoI)* [12]. AoI quantifies the time elapsed since the most recently delivered data or computational results were produced, providing a precise measure of information timeliness.

While numerous prior studies on MEC have focused on minimizing delay (e.g., [13], [14]), they often overlooked AoI, which is crucial for real-time applications. Here we highlight the huge difference between delay and AoI. Specifically, task delay measures the duration between task generation and task output reception. With less frequent updates (i.e., when tasks are generated in a lower frequency), task delays are naturally smaller due to reduced queuing delays from empty queues. In contrast, AoI considers both task delay and the output freshness. To minimize AoI for computational-intensive tasks, the update frequency must be balanced to reduce individual task delays while ensuring the freshness of the most recent task output. This difference between delay and AoI reveals a counterintuitive phenomenon in age-minimal scheduling: mobile devices may need to wait before generating new tasks after receiving a task output.

In this paper, we aim to answer the key question as follows.

Key Question. *How should mobile devices optimize their updating and offloading policies in real-time MEC systems in order to minimize AoI?*

Optimizing AoI in MEC systems requires a sophisticated scheduling policy for mobile devices, involving two key

Lyudong Jin and Meng Zhang are with the Zhejiang University—University of Illinois at Urbana–Champaign Institute, Zhejiang University, Haining 314400, China (e-mail: 3180101183@zju.edu.cn; mengzhang@intl.zju.edu.cn).

Ming Tang is with the Department of Computer Science and Engineering, Southern University of Science and Technology, Shenzhen 518000, China (e-mail: tangm3@sustech.edu.cn).

Jiayu Pan is with the School of Software Technology, Zhejiang University, Ningbo 315048, China (e-mail: jiayupan26@zju.edu.cn).

Hao Wang is with the Department of Data Science and AI, Faculty of Information Technology, Monash University, Melbourne, Victoria 3800, Australia (e-mail: hao.wang2@monash.edu).

Part of this paper was presented in AAAI-24 [1].

decisions: updating and offloading. The *updating* decision determines the interval between task completion and the initiation of the next task generation, while the *offloading* decision decides whether to process the task locally or offload it to a specific edge server. Given the success of multi-agent reinforcement learning (MARL) in MEC systems [15], we aim to design a fractional MARL framework with theoretical analysis and propose an asynchronous fractional multi-agent deep reinforcement learning (MADRL) to optimize the task scheduling policy. A few significant questions of our paper are presented as follows.

How to deal with the fractional nature of AoI objective in RL? Many prior works on MEC have explored offloading (e.g., [14], [16]–[19]) and some have considered AoI (e.g. [8], [18], [19]). However, they did not consider the fractional AoI objective, which improves data timeliness but introduces significant complexity and instability for RL due to its nonlinear nature. Consequently, real-time MEC systems require a fractional RL framework to address the fractional AoI objective.

How could we adapt the fractional framework to multi-agent scenario? Many MEC systems involve s decision-making processes among multiple mobile devices. Effectively addressing this multi-agent paradigm in MARL is important for task scheduling in multi-agent systems. However, the fractional framework for single agent cannot be directly adapted to the multi-agent scenario due to the increased complexity and inter-dependencies among agents. Thus, the MARL framework faces additional challenges in designing the fractional framework for the AoI objective.

How to address the asynchronous decision problem in real-time MEC systems? Traditional MADRL algorithms, such as multi-agent deep deterministic gradient descent (MADDPG) [20] assume that agents make decisions synchronously. However, in multi-agent MEC systems, each agent (mobile device) has different task update and processing durations, leading to asynchronous decision-making among agents. Traditional MADRL algorithms including QMIX [21] and MAPPO [22] would be inefficient to address the challenge of asynchronous control in MEC scheduling problem. Thus, addressing these challenges necessitates novel approaches that can effectively handle the asynchronous nature of agent interactions in MEC environments.

B. Solution Approaches and Contributions

In this paper, we address the aforementioned challenges and design an MARL algorithm to jointly optimize task updating and offloading policies for AoI in MEC systems. We model the multi-agent interaction as a semi-Markov game (SMG), where agents' state transitions and rewards depend on asynchronous actions. Our approach includes three steps. First, we propose a fractional RL framework based on Dinkelbach's fractional programming [23] for single-agent scenario. We then design a fractional MARL framework that incorporates Nash Q-learning [24] with fractional programming for multi-agent scenario. Finally, to handle asynchronous decision-making in SMG, we develop an asynchronous fractional MARL framework with an asynchronous trajectory collection mechanism.

Our main contributions are summarized as follows:

- *Joint Task Updating and Offloading Problem:* We formulate a joint task updating and offloading problem, accounting for the fractional nature of AoI, the multi-agent system and the asynchronous decision-making processes of mobile devices. *To the best of our knowledge, this is the first work designing multi-agent asynchronous policies for the joint updating and offloading optimization in age-minimal MEC.*
- Fractional RL Framework: We consider the scenario of single-agent task scheduling and propose a fractional RL framework that integrates RL with Dinkelbach's method. This methodology can adeptly handle fractional objectives within the RL paradigm and demonstrates a linear convergence rate.
- *Fractional MARL Framework:* To address the fractional objective challenge in a multi-agent scenario, we first consider a Markov game, where agents' state transitions and rewards depend on their joint actions. We propose a novel fractional MARL framework. Our framework guarantees the existence of a Nash equilibrium (NE) within our fractional framework. Furthermore, we prove that our algorithm can converge to the NE.
- *Asynchronous Fractional MADRL Algorithm:* We then propose a novel asynchronous fractional MADRL framework to minimize AoI and approximate the NE in SMG. Our framework integrates several key components as follows. First, we incorporate the dueling double deep Q-network (D3QN) and proximal policy optimization (PPO) into our fractional framework to handle hybrid action spaces. To address the asynchronous nature of SMGs, we implement a novel asynchronous trajectory collection mechanism. We also incorporate a recurrent neural network (RNN) to synthesize information and evaluate other agents' strategies. These enhancements enable our framework to approximate the NE in the asynchronous environment of SMG and effectively minimize AoI for MEC systems.
- *Performance Evaluation:* Our experimental evaluation demonstrates that the asynchronous fractional MADRL algorithm outperforms benchmarks. When compared with benchmarks, our proposed algorithm improves the average AoI by up to 52.6%. The experimental results validate that both the fractional framework and the asynchronous mechanism contribute to enhancing the overall system performance.

II. Literature Review

Mobile Edge Computing: Existing MEC research has explored various areas, including resource allocation [25], service placement [26], proactive caching [27], and task offloading [28]. Many studies have proposed RL-based approaches to optimize task delays in a centralized manner (e.g., [29], [30]) or in a decentralized manner (e.g., [14], [31]). *Despite the success in reducing the task delay, these approaches are NOT easily applicable to age-minimal MEC due to the challenges of fractional objective and asynchronous decision-making.*

Multi-Agent RL in MEC: Multi-Agent RL has been widely adopted in multi-agent approaches with decentralized manners in MEC systems. Li *et. al.* proposed a decentralized edge server grouping algorithm and achieved NE by proving it to be exact potential game [32]. Chen *et al.* addressed the task offloading in the information freshness-aware air-ground integrated multi-access edge computing by letting each non-cooperative mobile user behave independently with local conjectures utilizing double deep Q-network. Feng *et al.* utilized a gating threshold to intelligently choose between local and global observations and limit the information transmission for approximating Nash equilibrium in an anti-jamming Markov game [33]. However, these MARL approaches have not considered the fractional objective when reaching NE.

Age of Information: Kaul *et al.* first introduced AoI in [12]. Some recent studies have studied AoI in CPS (e.g., [34], [35]). The majority of works have focused on the optimization of AoI in queueing systems and wireless networks, assuming the availability of complete and known statistical information (see [36], [37]). The above studies analyzed single-device-single-server models and hence did not consider offloading. A few studies have investigated RL algorithms design to minimize AoI in various application scenarios, including wireless networks [38], Internet-of-Things [39], autonomous driving [8], vehicular networks [40], and UAV-aided networks [41]. They mainly focused on optimizing resource allocation and trajectory design. Some works considered AoI as the performance metric for task offloading in MEC and proposed RL-based approaches. For instance, Chen *et al.* in [19] considered AoI to capture the freshness of computation outcomes and proposed a multi-agent RL algorithm. *However, these works focused solely on designing task offloading policies without jointly optimizing updating policies. Note that none of these approaches have considered fractional RL and are difficult to directly address the problem in this pape.*

RL with Fractional Objectives: There is limited analysis on researches on RL with fractional objectives. Ren *et. al.* introduced fractional MDP [42]. Tanaka *et. al.* [43] further studied partially observed MDPs with fractional costs. However, these studies haven't extended to RL framework. Suttle *et al.* [44] proposed a two-timescale RL algorithm for fractional cost optimization. However, this method requires fixed reference states in Q-learning updates, which cannot be directly adapted to an asynchronous multi-agent environment.

Asynchronous Decision-Making MARL: Research on asynchronous decision-making in MARL is also limited. Chen et al. [45] proposed VarLenMARL in which each agent can have an independent time step with variable global system time length. Meanwhile, VarLenMARL maintains a synchronized delay-tolerant mechanism in which the agent can gather the padding data of the most up-to-date step of other agents. However, this approach becomes inefficient with a large number of agents and may neglect information from frequently deciding agents. Liang et al. [46] addressed these issues with ASM-PPO, which collected agent trajectories independently and trains using available agents at each time slot. However, ASM-PPO could also lose track of the correct decision-making order when the decision-making frequencies vary significantly. Therefore, this algorithm cannot be adapted to our task scheduling problem, which involves high variability in agents' decision-making.

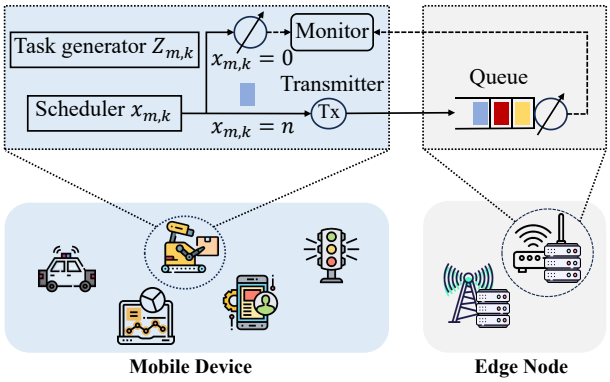

Fig. 1. An illustration of an MEC system with a mobile device $m \in \mathcal{M}$ and an edge server $n \in \mathcal{N}$ where the tasks offloaded by different mobile devices are represented using different colors.

III. System Model

In this section, we present the system model for MEC. We first introduce th device and edge server model. We then define the AoI in our MEC setting and formulate the task scheduling problem within a semi-Markov game framework.

In this MEC system model, we consider mobile devices $\mathcal{M} = \{1, 2, \cdots, M\}$ and edge servers $\mathcal{N} = \{1, 2, \cdots, N\}$ respectively, as shown in Fig. 1. We denote the set of tasks as $\mathcal{K} = \{1, \cdots, K\}$.

A. Device Model

As shown in Fig. 1, each mobile device m includes a task generator, a scheduler, a monitor, and a local processor. The generator produces computational tasks. The scheduler chooses to process them locally or offload to an edge server. After the edge server or local processor processes the task, the result is sent to the monitor and the generator then decides when to initiate a new task.

Generator: We consider a *generate-at-will* model, as in [47]–[51], where each mobile device's task generator determines when to generate the new task. Specifically, when task $k-1$ of mobile device $m \in \mathcal{M}$ is completed at $t'_{m,k-1}$, the task generator observes the latency $Y_{m,k}$ of task k and queue information of edge servers $\boldsymbol{q}(t'_{m,k-1})$. It then decides on $Z_{m,k}$, i.e., the waiting time before generating the *next* task k. We assume that edge servers share their load levels in response to mobile device queries. Since a generator produces a new task after the previous task is finished, the queue length is less than or equal to M, which incurs minimal signaling overheads. Let $a^{\mathrm{U}}_{m,k}$ denote the updating action for task k, i.e., $a^{\mathrm{U}}_{m,k} = Z_{m,k}$ and $\mathcal{A}^{\mathrm{U}} = \mathbb{R}^M$ be the updating action space. The generation time of task k is calculated as $t_{m,k} = t'_{m,k-1} + Z^k_m$. Notably, an optimal waiting strategy for updating can outperform a zero-wait policy, indicating that the waiting time $Z_{m,k}$ is not necessarily zero and should be optimized for efficiency [47].

Scheduler: When the generator produces task k at time $t_{m,k}$, the scheduler makes the offloading decision $x_{m,k} \in \{0\} \cup \mathcal{N}$ with the queue information $\boldsymbol{q}(t_{m,k})$ of edge servers[1]. Let $a^{\mathrm{O}}_{m,k}$ denote the action of task k from mobile device m. That is, $a^{\mathrm{O}}_{m,k} = x_{m,k}, k \in \mathcal{K}, m \in \mathcal{M}$. Let $\mathcal{A}^{\mathrm{O}} \in \{0\} \cup \mathcal{N}$ and π^{O}_m denote the offloading action space and the task offloading policy of mobile device $m \in \mathcal{M}$, respectively. For local processing on mobile device $m \in \mathcal{M}$, $\tau^{local}_{m,k}$ (in seconds) represents the processing time of task k. The value of $\tau^{local}_{m,k}$ depends on the task size and the real-time computational capacity of mobile device (e.g., whether the device is busy in processing tasks of other applications). For offloading task k to edge server $n \in \mathcal{N}$, $\tau^{tran}_{n,m,k}$ (in seconds) denotes the transmission latency of mobile device m. The value of $\tau^{tran}_{n,m,k}$ depends on the time-varying wireless channels. We assume that $\tau^{local}_{m,k}$ and $\tau^{tran}_{n,m,k}$ are random variables that follow exponential distributions, as in [31], [52], [53].

B. Edge Server Model

When a mobile device offloads the task to edge server $n \in \mathcal{N}$, the task is stored in a queue waiting for processing, as shown in Fig. 1. We assume the queue operates on a first-come-first-served (FCFS) basis [36]. We denote $\boldsymbol{q}(t) = (q_n(t), n \in \mathcal{N})$ as the queue lengths of all edge servers. Edge servers update their queue length information $\boldsymbol{q}(t)$ in two cases: when a task is completed or when a waiting period ends. Recall that a generator generates a new task only after the previous task has been processed, the queue length is less than or equal to M. Thus, the information to be sent can be encoded in $O(\log_2 M)$ bits with minimal signaling overheads. We denote $w^{edge,k}_{n,m}$ (in seconds) as the duration that task k of mobile device $m \in \mathcal{M}$ waits at the queue of edge server n. Let $\tau^{edge,k}_{n,m}$ (in seconds) denote the latency of edge server n for processing task k of mobile device m. We assume that $\tau^{edge,k}_{n,m}$ is a random variable following an exponential distribution i.e., $\tau^{edge}_{n,m,k} \sim Exp(\frac{C^{edge}_n}{l^k d^k})$. Here, C^{edge}_n is the processing capacity (in GHz) of edge n. Paramters l^k and d^k denotes the task size and task density of k respectively. In addition, the value of $w^{edge,k}_{n,m}$ depends on the processing times of the tasks ahead in the queue, which are possibly offloaded by other mobile devices. Additionally, these offloading information cannot be directly observed by mobile device m.

C. Age of Information

For mobile device m, the AoI at global clock T [36] is defined by

$$\Delta_m(t) = t - T_m(t), \quad \forall m \in \mathcal{M}, t \geq 0, \tag{1}$$

where $T_m(t) \triangleq \mathrm{maximize}_k(t_{m,k} | t'_{m,k} \leq t)$ stands for the time stamp of the most recently completed task.

[1]Under the system model in Section III, observing the queue lengths of edge servers is sufficient for mobile devices to learn their offloading policies. Under a more complicated system (e.g., with device mobility), additional state information may be necessary. However, our proposed RL-based framework remain applicable with an extended state vector.

The overall duration to complete task k is denoted by $Y_{m,k} \triangleq t'_{m,k} - t_{m,k}$. Therefore,

$$Y_{m,k} = \begin{cases} \tau^{local}_{m,k}, & x_{m,k} = 0, \\ \tau^{tran}_{n,m,k} + w^{edge}_{n,m,k} + \tau^{edge}_{n,m,k}, & x_{m,k} = n \in \mathcal{N}. \end{cases} \tag{2}$$

We consider a deadline $\bar{Y}$ (in seconds). Tasks not completed within $\bar{Y}$ seconds will be dropped [14], [54]. Meanwhile, the AoI keeps increasing until the next task is completed.

We define the trapezoid area associated with time interval $[t_{m,k}, t_{m,k+1}]$:

$$\begin{aligned} &A(Y_{m,k}, Z_{m,k+1}, Y_{m,k+1}) \\ \triangleq &\frac{1}{2}(Y_{m,k} + Z_{m,k+1} + Y_{m,k+1})^2 - \frac{1}{2}(Y_{m,k+1})^2, \end{aligned} \tag{3}$$

where $Z_{m,k+1}$ denotes the updating interval before generating next task $k+1$. Based on (3), we can characterize the objective of mobile device m, i.e., to minimize the time-average AoI of each device $m \in \mathcal{M}$:

$$\Delta^{(ave)}_m \triangleq \liminf_{K \to \infty} \frac{\sum_{k=0}^{K} \mathbb{E}[A(Y_{m,k}, Z_{m,k+1}, Y_{m,k+1})]}{\sum_{k=0}^{K} \mathbb{E}[Y_{m,k} + Z_{m,k+1}]}, \tag{4}$$

where $\mathbb{E}[\cdot]$ is the expectation with respect to decisions made according to certain policies, which will be elaborated upon in the subsequent sections.

D. Game Formulation

In MEC systems, mobile devices make updating and offloading decisions asynchronously due to variable transition times. These transition times fluctuate based on scheduling strategies and edge workloads. Given that the current MARL framework is designed for synchronous decision-making processes, it is not suitable for application in this context. To address this challenge, we model the real-time MEC scheduling problem as an SMG. An SMG extends Markov decision processes to multi-agent systems with variable state transition times. Thus, this framework can address asynchronous decision-making in MEC systems.

The game is defined as $(\mathcal{M}, \mathcal{S}, \mathcal{A}, P_{\mathcal{S}}, P_F, \mu_0)$, where $\mathcal{M}$ is the set of mobile devices. A state $\boldsymbol{s} \in \mathcal{S}$ is expressed as $\boldsymbol{s} \triangleq ((I_m)_{m \in \mathcal{M}}, (\boldsymbol{q}(t_m))_{m \in \mathcal{M}}, (Y_m)_{m \in \mathcal{M}}), \boldsymbol{s} \in \mathcal{S}$, where $(I_m)_{m \in \mathcal{M}}$ denotes the decision indicators, specifying whether each mobile device $m \in \mathcal{M}$ needs to take offloading action a^{O}_m, updating action a^{U}_m or make no decisions. The state space $\mathcal{S}$ is defined as $\mathbb{N}^N \times \mathbb{N}^N \times \mathbb{R}^M$. The action space $\mathcal{A}$ is defined as $\mathcal{A}^{\mathrm{U}} \times \mathcal{A}^{\mathrm{O}}$. Specifically, an action $\boldsymbol{a} \in \mathcal{A}$ consists of its task updating action $\boldsymbol{a}^{\mathrm{U}}$ and task offloading action $\boldsymbol{a}^{\mathrm{O}}$. We define the set of admissible triplets as $\mathcal{H} = \{(\boldsymbol{s}, \boldsymbol{a}) | \boldsymbol{s} \in \mathcal{S}, \boldsymbol{a} \in \mathcal{A}\}$. Let $\mathbb{P}(\mathcal{S})$ denote the collection of probability distributions over space $\mathcal{S}$. The transition function of the game is $P_{\mathcal{S}} : \mathcal{H} \to \mathbb{P}(\mathcal{S})$ and the stochastic kernel determining the transition time distribution is $P_F : \mathcal{H} \times \mathcal{S} \to \mathbb{P}(\mathbb{R}^+)$. Additionally, μ_0 denotes the initial state distribution.

We define policy space for semi-Markov game as $\Pi \triangleq \{\boldsymbol{\pi} = (\boldsymbol{\pi}_m)_{m \in \mathcal{M}}\}$, where each policy $\boldsymbol{\pi}_m = (\boldsymbol{\pi}^{\mathrm{U}}_m, \boldsymbol{\pi}^{\mathrm{O}}_m)$ including

both the updating and offloading policies of single mobile device m. We define the expected long-term discounted AoI of mobile device m as

$$\mathbb{E}_{\boldsymbol{\pi}}[\Delta_m] \triangleq \mathop{\mathbb{E}}_{\boldsymbol{s}_0\sim\mu_0}\left\{\frac{\sum_{k=0}^{\infty}\delta^k\mathbb{E}_{\boldsymbol{\pi}}[A(Y_{m,k},Z_{m,k+1},Y_{m,k+1})]}{\sum_{k=0}^{\infty}\delta^k\mathbb{E}_{\boldsymbol{\pi}}[Y_{m,k}+Z_{m,k+1}]}\right\}, \tag{5}$$

where $\delta\in(0,1)$ is a discount factor. We have the objective with the initial state $\boldsymbol{s}_0$ under initial distribution μ_0. For simplicity, we drop the notation $\mathop{\mathbb{E}}_{\boldsymbol{s}_0\sim\mu_0}[\cdot]$, which is by default unless stated otherwise in the following. Note that the discounted AoI form facilitates the application of AoI optimization in RL and MARL frameworks that utilize discounted cost functions. Additionally, as δ approaches 1, the discounted AoI (5) approximates the undiscounted AoI function (4). We take the expectation $\mathbb{E}_{\boldsymbol{\pi}}[\cdot]$ over policy $\boldsymbol{\pi}$ and the time-varying system parameters, e.g., the time-varying processing duration as well as the edge load dynamics. We define the Nash equilibrium $\boldsymbol{\pi}^\star=(\boldsymbol{\pi}_m^\star)_{m\in\mathcal{M}}$ for our task scheduling problem as follows.

Definition 1 (Nash Equilibrium)**.** *In stochastic game G, a Nash equilibrium point is a tuple of policies* $(\boldsymbol{\pi}_1^\star,\ldots,\boldsymbol{\pi}_m^\star)$ *of cost functions such that for all* $m\in\mathcal{M}$ *we have,*

$$\mathbb{E}_{\boldsymbol{\pi}_m^\star,\boldsymbol{\pi}_{-m}^\star}[\Delta_m]\le\mathbb{E}_{\boldsymbol{\pi}_m,\boldsymbol{\pi}_{-m}^\star}[\Delta_m]. \tag{6}$$

For each mobile device $m\in\mathcal{M}$, given the fixed stationary policies $\boldsymbol{\pi}_{-m}^\star$, the best response in our real-time MEC scheduling problem is defined as

$$\boldsymbol{\pi}_m^\star=\arg\mathop{\text{minimize}}_{\boldsymbol{\pi}_m}\ \mathbb{E}_{\boldsymbol{\pi}_m,\boldsymbol{\pi}_{-m}^\star}[\Delta_m]. \tag{7}$$

Solving (7) is challenging due to the following reasons. First, the fractional objective introduces a major challenge in obtaining the optimal policy for conventional RL algorithms due to its non-linear nature. Second, the multi-agent environment introduces complex dynamics from interactions between edge servers and mobile devices. Third, the continuous time nature, stochastic state transitions, and asynchronous decision-making in SMG pose significant challenges in directly applying conventional game-theoretic methodologies.

In the following sections, we first analyze a simplified version of the single-agent fractional RL framework. This framework establishes a robust theoretical foundation and serves as a benchmark for subsequent experiments. We then extend our theoretical analysis of our fractional framework to multi-agent scenarios, which is closer to SMG and piratical dynamics. Finally, we propose the fractional MADRL algorithm in asynchronous setting for SMG, which matches the practical dynamics of real-time MEC systems.

IV. Fractional Single-Agent RL Framework

For foundational theoretical analysis, we first consider a fractional single-agent RL framework. We design a fractional MDP and propose fractional Q-learning a algorithm. We provide analysis of the linear convergence for this algorithm. We formulate the problem as follows.

A. Single-Agent Problem Formulation

The objective for single-agent MEC system can be expressed as

$$\boldsymbol{\pi}_m^*=\arg\mathop{\text{minimize}}_{\boldsymbol{\pi}_m}\ \mathbb{E}_{\boldsymbol{\pi}_m}[\Delta_m], \tag{8}$$

where we focus on the policy of agent m alone, compared with (7). We study the general fractional MDP framework and drop the index m in the rest of this section.

We introduce a fractional RL framework to address Problem (8). Specifically, we first reformulate Problem (8). We then introduce a fractional RL framework and propose a fractional Q-learning algorithm with provable convergence guarantees.

B. Dinkelbach's Reformulation

To solve Problem (8), we consider the Dinkelbach's reformulation. Specifically, we define a reformulated AoI in a discounted fashion:

$$\begin{aligned}\mathbb{E}_{\boldsymbol{\pi}}[\Delta',\gamma]\triangleq\sum_{k=0}^{\infty}\delta^k\mathbb{E}_{\boldsymbol{\pi}}[&A(Y_k,Z_{k+1},Y_{k+1})\\&-\gamma(Y_k+Z_{k+1})],\forall\gamma\ge0.\end{aligned} \tag{9}$$

Let γ^* be the optimal value of Problem (8). By leveraging Dinkelbach's method [23], we reformulate the problem as follows.

Lemma 1 (Asymptotic Equivalence [23])**.** *Problem* (8) *is equivalent to the following reformulated problem:*

$$\boldsymbol{\pi}^*=\arg\mathop{\text{minimize}}_{\boldsymbol{\pi}}\ \mathbb{E}_{\boldsymbol{\pi}}[\Delta',\gamma^*], \tag{10}$$

where $\boldsymbol{\pi}^*$ *is the optimal solution to Problem* (8)*.*

Since $\mathbb{E}_{\boldsymbol{\pi}}[\Delta',\gamma^*]\ge0$ for any π and $\mathbb{E}_{\boldsymbol{\pi}^*}[\Delta',\gamma^*]=0$, $\boldsymbol{\pi}^*$ is also optimal for the Dinkelbach reformulation. This implies that the reformulation equivalence is also established for our stationary policy space.

C. Fractional MDP

We then extend the standard MDP to a fractional form, laying the goundwork to more complex and practical setting in Markov game.

A fractional MDP is defined as $(\mathcal{S},\mathcal{A},P,c_N,c_D,Pr,\delta,\mu_0)$, where $\mathcal{S}$ and $\mathcal{A}$ are the finite sets of states and actions, respectively; Pr is the state transition distribution; c_N and c_D are the fractional costs, δ is a discount factor, and $\mu_0=\{\mu_0(\boldsymbol{s})\}_{\boldsymbol{s}\in\mathcal{S}}$ denotes the initial global state distribution. We use $\mathcal{Z}$ to denote the joint state-action space, i.e., $\mathcal{Z}\triangleq\mathcal{S}\times\mathcal{A}$. We define the instant fractional costs at task k as

$$c_N(\boldsymbol{s}_k,\boldsymbol{a}_k)=A(Y_k,Z_{k+1},Y_{k+1}), \tag{11}$$

$$c_D(\boldsymbol{s}_k,\boldsymbol{a}_k)=Y_k+Z_{k+1}. \tag{12}$$

From Lemma 1, Problem (8) has the equivalent Dinkelbach's reformulation:

$$\boldsymbol{\pi}^*=\arg\mathop{\text{minimize}}_{\boldsymbol{\pi}}\lim_{K\to\infty}\mathbb{E}_{\boldsymbol{\pi}}\left[\sum_{k=0}^{K}\delta^k(c_N-\gamma^*c_D)\right], \tag{13}$$

Algorithm 1 Fractional Q-Learning (FQL)

for episode $i = 0, 1, \cdots, I$ **do**
  Initialize $\boldsymbol{s}_0$;
  for task $k = 0, 1, \cdots, K$ **do**
    Observe the next state $\boldsymbol{s}_m(t+1)$;
    Observe a set of costs $\{c_{N,k}, c_{D,k}\}$;
    Submit $(\boldsymbol{s}_k, \boldsymbol{a}_k, c_{N,k}, c_{D,k}, \boldsymbol{s}_{k+1})$;
  end for
  $\gamma_{i+1} = N_{\gamma_i}(\boldsymbol{s}, \boldsymbol{a}_i)/D_{\gamma_i}(\boldsymbol{s}, \boldsymbol{a}_i)$, where $\boldsymbol{a}_i = \arg\max_{\boldsymbol{a}} Q_{\gamma_i}(\boldsymbol{s}, \boldsymbol{a})$.
end for

where we can see from Lemma 1 that γ^* satisfies

$$\gamma^* = \underset{\boldsymbol{\pi}}{\text{minimize}} \lim_{K\to\infty} \frac{\mathbb{E}_{\boldsymbol{\pi}}\left[\sum_{k=0}^{K} \delta^k c_N\right]}{\mathbb{E}_{\boldsymbol{\pi}}\left[\sum_{k=0}^{K} \delta^k c_D\right]}. \tag{14}$$

Note that Problem (13) is a classical MDP problem, including an immediate cost $c_N(\boldsymbol{s}, \boldsymbol{a}) - \gamma^* c_D(\boldsymbol{s}, \boldsymbol{a})$. Thus, we can apply a traditional RL algorithm to solve such a reformulated problem, such as Q-Learning or its variants (e.g., SQL in [55]).

However, the optimal quotient coefficient γ^* and the transition distribution P are not known *a priori*. Therefore, we design an algorithm that combines fractional programming and reinforcement learning to solve Problem (13) for a given γ and seek the value of γ^*. To achieve this, we start by introducing the following definitions.

Given a quotient coefficient γ, the optimal Q-function is

$$Q^*_\gamma(\boldsymbol{s}, \boldsymbol{a}) \triangleq \underset{\boldsymbol{\pi}}{\text{minimize}}\ Q^{\boldsymbol{\pi}}_\gamma(\boldsymbol{s}, \boldsymbol{a}),\ \forall (\boldsymbol{s}, \boldsymbol{a}) \in \mathcal{Z}, \tag{15}$$

where $Q^{\boldsymbol{\pi}}_\gamma(\boldsymbol{s}, \boldsymbol{a})$ is the action-state function that satisfies the following Bellman's equation: for all $(\boldsymbol{s}, \boldsymbol{a}) \in \mathcal{Z}$,

$$Q^{\boldsymbol{\pi}}_\gamma(\boldsymbol{s}, \boldsymbol{a}) \triangleq c_N(\boldsymbol{s}, \boldsymbol{a}) - \gamma c_D(\boldsymbol{s}, \boldsymbol{a}) + \delta \mathbb{E}_{Pr}\left[Q^{\boldsymbol{\pi}}_\gamma(\boldsymbol{s}', \boldsymbol{a})\right], \tag{16}$$

where $\mathbb{E}_{Pr}$ is a concise notation for $\mathbb{E}_{\boldsymbol{s}'\sim Pr(\cdot|\boldsymbol{s},\boldsymbol{a})}$. In addition, we can further decompose the optimal Q-function in (15) into the following two parts: $Q^*_\gamma(\boldsymbol{s}, \boldsymbol{a}) = N_\gamma(\boldsymbol{s}, \boldsymbol{a}) - \gamma D_\gamma(\boldsymbol{s}, \boldsymbol{a})$ and, for all $(\boldsymbol{s}, \boldsymbol{a}) \in \mathcal{Z}$,

$$N_\gamma(\boldsymbol{s}, \boldsymbol{a}) = c_N(\boldsymbol{s}, \boldsymbol{a}) + \delta \mathbb{E}_{Pr}\left[N_\gamma(\boldsymbol{s}', \boldsymbol{a})\right], \tag{17}$$

$$D_\gamma(\boldsymbol{s}, \boldsymbol{a}) = c_D(\boldsymbol{s}, \boldsymbol{a}) + \delta \mathbb{E}_{Pr}\left[D_\gamma(\boldsymbol{s}', \boldsymbol{a})\right]. \tag{18}$$

D. Fractional Q-Learning Algorithm

In this subsection, we present a Fractional Q-Learning (FQL) algorithm (see Algorithm 1). The algorithm consisting of an inner loop with E episodes and an outer loop. The key idea is to approximate the Q-function Q^*_γ using Q_i in the inner loop, while iterating over the sequence $\{\gamma_i\}$ in the outer loop.

A notable innovation in Algorithm 1 is the design of the stopping condition, which ensures that the uniform approximation errors of Q_i shrink progressively. This allows us to adapt the convergence proof from [23] to our inner loop, while proving the linear convergence rate of $\{\gamma_i\}$ in the outer loop. Importantly, this design does not increase the time complexity of the inner loop.

We describe the details of the inner loop and the outer loop procedures of Algorithm 1 in the following:

- *Inner loop*: For each episode i, given a quotient coefficient γ_i, we perform an (arbitrary) Q-Learning algorithm (as the Speedy Q-Learning in [55]) to approximate function $Q^*_\gamma(\boldsymbol{s}, \boldsymbol{a})$ by $Q_i(\boldsymbol{s}, \boldsymbol{a})$. Let $\boldsymbol{s}_0$ denote the initial state of any episode, and $\boldsymbol{a}_i \triangleq \arg\max_{\boldsymbol{a}} Q_i(\boldsymbol{s}_0, \boldsymbol{a})$ for all $i \in [E] \triangleq \{1, ..., E\}$. We consider a *stopping condition*

$$\epsilon_i < -\alpha Q_i(\boldsymbol{s}_0, \boldsymbol{a}_i),\ \forall i \in [E], \tag{19}$$

  where $\alpha > 0$ is the error scaling factor. This stopping condition ensures the algorithm being terminated in each episode i with a bounded *uniform approximation error*: $\|Q^*_\gamma - Q_i\| \le \epsilon_i,\ \forall i \in [E]$. Operator $\|\cdot\|$ is the supremum norm, which satisfies $\|g\| \triangleq \max_{(\boldsymbol{s},\boldsymbol{a})\in\mathcal{Z}} g(\boldsymbol{s}, \boldsymbol{a})$. Specifically, we obtain $Q_i(\boldsymbol{s}_0, \boldsymbol{a}_i)$, $N_i(\boldsymbol{s}_0, \boldsymbol{a}_i)$, and $D_i(\boldsymbol{s}_0, \boldsymbol{a}_i)$, which satisfy,

$$Q_i(\boldsymbol{s}_0, \boldsymbol{a}_i) = N_i(\boldsymbol{s}_0, \boldsymbol{a}_i) - \gamma_i D_i(\boldsymbol{s}_0, \boldsymbol{a}_i). \tag{20}$$

- *Outer loop:* We update the quotient coefficient:

$$\gamma_{i+1} = \mathop{\mathbb{E}}_{\boldsymbol{s}_0\sim\mu_0}\left[\frac{N_i(\boldsymbol{s}_0, \boldsymbol{a}_i)}{D_i(\boldsymbol{s}_0, \boldsymbol{a}_i)}\right], \quad \forall i \in [E], \tag{21}$$

  which will be shown to converge to the optimal value γ^*.

E. Convergence Analysis

We present the time complexity analysis of inner loop and the convergence results of our proposed FQL algorithm (Algorithm 1) as follows.

1) Time Complexity of the inner loop: Although as $\{Q_i(\boldsymbol{s}_0, \boldsymbol{a}_i)\}$ is convergent to 0 and hence $\epsilon_i < -\alpha Q_i$ is getting more restrictive as i increases, the steps needed T_i in Algorithm 1 keep to be finite without increasing over episode i. See Appendix A in detail.

2) Convergence of FQL algorithm: We then analyzing the convergence of FQL algorithm:

Theorem 1 (Linear Convergence of Fractional Q-Learning)**.** *If the uniform approximation error $\|Q^*_{\gamma_i} - Q_i\| \le \epsilon_i$ holds with $\epsilon_i < -\alpha Q_i(\boldsymbol{s}_0, \boldsymbol{a}_i)$ for some $\alpha \in (0, 1)$ and for all $i \in [E]$, then the sequence $\{\gamma_i\}$ generated by Algorithm 1 satisfies*

$$\frac{\gamma_{i+1} - \gamma^*}{\gamma_i - \gamma^*} \in (0, 1),\ \forall i \in [E] \text{ and } \lim_{i\to\infty} \frac{\gamma_{i+1} - \gamma^*}{\gamma_i - \gamma^*} = \alpha. \tag{22}$$

That is, $\{\gamma_i\}$ converges to γ^* linearly.

While the convergence proof in [23] requires to obtain the *exact* solution in each episode, Theorem 1 generalizes this result to the case where we only obtain an *approximated (inexact)* solution in each episode. In addition to the proof techniques in [23] and [55], our proof techniques include induction and exploiting the convexity of $Q_i(\boldsymbol{s}, \boldsymbol{a})$. We present a proof sketch of Theorem 1 in Appendix B.

The significance of Theorem 1 is two-fold. First, Theorem 1 shows that Algorithm 1 achieves a linear convergence rate, even though it only attains an approximation of $Q^*_\gamma(\boldsymbol{s}, \boldsymbol{a})$. Second, (19) is a well-behaved stopping condition.

V. Fractional MARL Framework

In this section, we propose a fractional MARL framework, extending our fractional framework from the single-agent scenario to the multi-agent one. We first introduce a Markov game for our task scheduling problem. We then develop a fractional framework including fractional sub-games to address the fractional objective challenge. Finally, we propose the fractional Nash q-learning algorithm and analyze the convergence of this algorithm to Nash equilibrium.

A. Markov Game Formulation

We study our problem in in a multi-agent scenario and introduce the task scheduling Markov game.

The task scheduling Markov game is defined as: $G = (M, \mathcal{S}, \mathcal{A}, \{c_{N,m}\}_{m=1}^{M}, \{c_{D,m}\}_{m=1}^{M}, Pr, \delta, \mu_0)$ where M is the number of agents, $\mathcal{S}$ and $\mathcal{A}$ represent the state space and action space, respectively, $Pr(\boldsymbol{s}'|\boldsymbol{s}, \boldsymbol{a})$ denotes the state transition probability, $\delta \in (0, 1)$ is discounted factor, and μ_0 denotes the initial state distribution.

We define the instant fractional costs at task k of mobile device m as

$$c_{N,m}(\boldsymbol{s}_k, \boldsymbol{a}_k) = A(Y_{m,k}, Z_{m,k+1}, Y_{m,k+1}), \tag{23}$$

$$c_{D,m}(\boldsymbol{s}_k, \boldsymbol{a}_k) = Y_{m,k} + Z_{m,k+1}. \tag{24}$$

Following the definition of discounted AoI in (5), we define the fractional long-term discounted cost for mobile device m as

$$V_m(\boldsymbol{s}, \boldsymbol{\pi}) = \frac{\mathbb{E}_{\boldsymbol{\pi}}\left[\sum_{k=0}^{\infty} \delta^k c_{N,m}(\boldsymbol{s}_k, \boldsymbol{a}_k) \middle| \boldsymbol{s}_0 = \boldsymbol{s}\right]}{\mathbb{E}_{\boldsymbol{\pi}}\left[\sum_{k=0}^{\infty} \delta^k c_{D,m}(\boldsymbol{s}_k, \boldsymbol{a}_k) \middle| \boldsymbol{s}_0 = \boldsymbol{s}\right]}, \tag{25}$$

where $\boldsymbol{\pi} = (\boldsymbol{\pi}_m, \boldsymbol{\pi}_{-m})$ represent the policies of mobile device m and other agents that determine actions, and $\mathbb{E}_{\boldsymbol{\pi}}$ is the expectation regarding transition dynamic given stationary control policy $\boldsymbol{\pi}$. Note that (25) approximates the un-discounted function when δ approaches 1 [56]. Specifically, an NE is a tuple of policies $\boldsymbol{\pi}^\star = (\boldsymbol{\pi}_m^\star, \boldsymbol{\pi}_{-m}^\star)$ of game G. For each mobile $m \in \mathcal{M}$, given the fixed stationary policies $\boldsymbol{\pi}_{-m}^\star$, the fractional objective can be expressed as:

$$\boldsymbol{\pi}_m^\star = \arg\underset{\boldsymbol{\pi}_m}{\text{minimize}}\ V_m(\boldsymbol{s}, \boldsymbol{\pi}_m, \boldsymbol{\pi}_{-m}^\star), \forall \boldsymbol{s} \in \mathcal{S}. \tag{26}$$

Lemma 2 guarantees the existence of an NE in game G.

Lemma 2. *For the multi-player stochastic game with expected long-term discounted costs, there always exists a Nash equilibrium in stationary polices, where the probability of taking an action remains constant throughout the game [57].*

B. Fractional Sub-Game

To deal with the fractional objective (26) for NE, we reformulated our game into iterative fractional sub-games based on Dinkelbach method [23] in this subsection.

First, we define sub-game $G_{\boldsymbol{\gamma}}$ with fractional coefficients $\boldsymbol{\gamma}$ for fractional sub-games as follows.

Definition 2 (Fractional Sub-Game)**.** *The fractional sub-game is defined as $G_{\boldsymbol{\gamma}} = (M, \mathcal{S}, \mathcal{A}, \{c_{N,m}\}_{m=1}^{M}, \{c_{D,m}\}_{m=1}^{M}, \delta, \boldsymbol{\gamma})$, where $\boldsymbol{\gamma} = \{\gamma_1, \cdots, \gamma_M\}$ are the set of fractional coefficients. Each γ_m is specific to mobile device m. These coefficients are used in the optimization process for the fractional sub-game.*

The fractional discounted cost value functions of sub-game is denoted as $\boldsymbol{V}_{\boldsymbol{\gamma}}(\boldsymbol{s}) := [V_{\gamma_m}(\boldsymbol{s})]_{m \in \mathcal{M}}$, then the fractional cost function of mobile device m can be defined as:

$$V_{\gamma_m}(\boldsymbol{s}, \boldsymbol{\pi}) = (1-\delta)\cdot \mathbb{E}_{\boldsymbol{\pi}}\left\{\sum_{k=0}^{\infty} \delta^k [c_{N_m}(\boldsymbol{s}_k, \boldsymbol{a}_k) - \gamma_m c_{D_m}(\boldsymbol{s}_k, \boldsymbol{a}_k)] \middle| \boldsymbol{s}_0 = \boldsymbol{s}\right\}, \tag{27}$$

where $\boldsymbol{s}_k, \boldsymbol{a}_k$ are the global state and action at task k. In sub-game $G_{\boldsymbol{\gamma}}$, each mobile device m aims to find its best response $\boldsymbol{\pi}_m^\star$. With policies of other agents $\boldsymbol{\pi}_{-m}^\star$ fixed, the best response of mobile device m minimizes its cost value V_{γ_m} for any given global system state $\boldsymbol{s} \in \mathcal{S}$. The objective is formulated as:

$$\boldsymbol{\pi}_m^\star = \arg\underset{\boldsymbol{\pi}_m}{\text{minimize}}\ V_{\gamma_m}(\boldsymbol{s}, \boldsymbol{\pi}_m, \boldsymbol{\pi}_{-m}^\star), \forall \boldsymbol{s} \in \mathcal{S}. \tag{28}$$

Lemma 2 ensures the existence of an NE in sub-game $G_{\boldsymbol{\gamma}}$. For brevity, we denote the optimal state-value function as $V_{\gamma_m}^\star(\boldsymbol{s}) = V_{\gamma_m}(\boldsymbol{s}, \boldsymbol{\pi}_m^\star, \boldsymbol{\pi}_{-m}^\star), \forall \boldsymbol{s} \in \mathcal{S}$, where $(\boldsymbol{\pi}_m^\star, \boldsymbol{\pi}_{-m}^\star)$ is the NE of sub-game $G_{\boldsymbol{\gamma}}$.

Thus, we propose a fractional Nash Q-Learning algorithm based on the iterative fractional sub-games and show its convergence in the rest of this section.

C. Fractional Nash Q-Learning Algorithm

We introduce the Fractional Nash Q-Learning (FNQL) algorithm in Algorithm 2. This algorithm includes two loops: *1)* an inner loop to obtain NE of sub-game $G_{\boldsymbol{\gamma}}$, and *2)* an outer loop to iterate $\boldsymbol{\gamma}$ until convergence. The key idea is to iterate sub-game $G_{\boldsymbol{\gamma}}$ and attain the NE of Markov game G when $\boldsymbol{\gamma}$ converges.

1) Inner Loop: Following [58], we first define the Nash operator $\mathcal{N}$ as follows:

Definition 3. *Consider a collection of M functions that can achieve a Nash equilibrium $\boldsymbol{\pi}^\star$, denoted as $\boldsymbol{f}(\boldsymbol{a}) = [f_m(\boldsymbol{a}_m, \boldsymbol{a}_{-m})]_{m \in \mathcal{M}}$. We introduce the Nash operator $\underset{\boldsymbol{a} \in \mathcal{A}}{\mathbb{N}}$, which maps the collections of functions into the values with their corresponding Nash equilibrium values $\boldsymbol{a}^\star$ as*

$$\underset{\boldsymbol{a} \in \mathcal{A}}{\mathbb{N}} \boldsymbol{f}(\boldsymbol{a}) = \mathbb{E}_{\boldsymbol{a} \sim \boldsymbol{\pi}^\star}[\boldsymbol{f}(\boldsymbol{a})], \tag{29}$$

where $\boldsymbol{\pi}^\star = (\boldsymbol{\pi}_m^\star, \boldsymbol{\pi}_{-m}^\star)$ satisfies

$$\mathbb{E}_{\boldsymbol{a} \sim (\boldsymbol{\pi}_m^\star, \boldsymbol{\pi}_{-m}^\star)}[f(\boldsymbol{a})] \leq \mathbb{E}_{\boldsymbol{a} \sim (\boldsymbol{\pi}_m, \boldsymbol{\pi}_{-m}^\star)}[f(\boldsymbol{a})], \forall m \in \mathcal{M}. \tag{30}$$

For sub-game $G_{\boldsymbol{\gamma}}$, the optimization of best response (28) utilize an instant cost, given by $c_{N_m}(\boldsymbol{s}, \boldsymbol{a}) -$

Algorithm 2 Fractional Nash Q-Learning (FNQL)

1: **repeat**
2: **for** task $k \in \mathcal{T}$ **do**
3: Initialize $\boldsymbol{s}_0$;
4: Choose action $\boldsymbol{a}$;
5: Observe $\boldsymbol{c}_N, \boldsymbol{c}_D, \boldsymbol{a}$, and $\boldsymbol{s}'$;
6: Update $\boldsymbol{Q}_{\boldsymbol{\gamma}}$ by (32);
7: **end for**
8: Update γ_m by (36) for all $m \in \mathcal{M}$;
9: **until** $\overline{\boldsymbol{N}}_{\boldsymbol{\gamma}}(\boldsymbol{s}_0) - \boldsymbol{\gamma}^\star \overline{\boldsymbol{D}}_{\boldsymbol{\gamma}}(\boldsymbol{s}_0) = 0$.

$\gamma_m c_{D_m}(\boldsymbol{s}, \boldsymbol{a}), \forall m \in \mathcal{M}$. To solve this optimization, we apply the traditional MARL algorithm Nash Q-learning [24]. We define the Nash Q-function with $\boldsymbol{\gamma}$ as:

$$\begin{aligned}\boldsymbol{Q}_{\boldsymbol{\gamma}}(\boldsymbol{s}, \boldsymbol{a}) \triangleq & \boldsymbol{c}_N(\boldsymbol{s}, \boldsymbol{a}) - \boldsymbol{\gamma} \odot \boldsymbol{c}_D(\boldsymbol{s}, \boldsymbol{a}) \\ & + \delta \mathbb{E}_{Pr}\left[\underset{\boldsymbol{a} \in \mathcal{A}}{\mathbb{N}} \boldsymbol{Q}_{\boldsymbol{\gamma}}(\boldsymbol{s}, \boldsymbol{a})\right], \end{aligned} \tag{31}$$

where we denote $\boldsymbol{c_N}(\boldsymbol{s}, \boldsymbol{a}) = [c_{N_m}(\boldsymbol{s}, \boldsymbol{a})]_{m \in \mathcal{M}}$, $\boldsymbol{c_D}(\boldsymbol{s}, \boldsymbol{a}) = [c_{D_m}(\boldsymbol{s}, \boldsymbol{a})]_{m \in \mathcal{M}}$ $\mathbb{E}_{Pr}$ is a concise notation for $\mathbb{E}_{\boldsymbol{s}' \sim Pr(\cdot|\boldsymbol{s}, \boldsymbol{a})}$. In the inner loop, we update Q-function of mobile device $m \in \mathcal{M}$ at task k by

$$\begin{aligned}\boldsymbol{Q}_{\boldsymbol{\gamma}}^{k+1}(\boldsymbol{s}, \boldsymbol{a}) = & (1-\lambda)\boldsymbol{Q}_{\boldsymbol{\gamma}}^{k}(\boldsymbol{s}, \boldsymbol{a}) + \lambda \{\boldsymbol{c}_N(\boldsymbol{s}, \boldsymbol{a}) - \boldsymbol{\gamma} \odot \boldsymbol{c}_D(\boldsymbol{s}, \boldsymbol{a}) \\ & + \delta \mathbb{E}_{Pr}\left[\underset{\boldsymbol{a} \in \mathcal{A}}{\mathbb{N}} \boldsymbol{Q}_{\boldsymbol{\gamma}}(\boldsymbol{s}', \boldsymbol{a})\right]\Big\}, \end{aligned} \tag{32}$$

where λ is the learning rate.

Then, let $\boldsymbol{Q}_{\boldsymbol{\gamma}}(\boldsymbol{s}, \boldsymbol{a}) = [Q_{\gamma_m}(\boldsymbol{s}, \boldsymbol{a})]_{m \in \mathcal{M}}$ be the collection of Q-functions. As in [58], $\boldsymbol{V}_{\boldsymbol{\gamma}}^\star(\boldsymbol{s}) = \underset{\boldsymbol{a} \in \mathcal{A}}{\mathbb{N}} \boldsymbol{Q}_{\boldsymbol{\gamma}}(\boldsymbol{s}, \boldsymbol{a})$. The Nash-Bellman equation can be expressed as

$$\boldsymbol{V}_{\boldsymbol{\gamma}}^\star(\boldsymbol{s}) = \underset{\boldsymbol{a} \in \mathcal{A}}{\mathbb{N}} \left\{\boldsymbol{c_N}(\boldsymbol{s}, \boldsymbol{a}) - \boldsymbol{\gamma} \odot \boldsymbol{c_D}(\boldsymbol{s}, \boldsymbol{a}) + \delta \mathbb{E}_{Pr}\left[\boldsymbol{V}_{\boldsymbol{\gamma}}^\star(\boldsymbol{s}')\right]\right\}. \tag{33}$$

We define $\overline{\boldsymbol{N}}_{\boldsymbol{\gamma}}^\star(\boldsymbol{s})$, $\overline{\boldsymbol{D}}_{\boldsymbol{\gamma}}^\star(\boldsymbol{s})$ as follows

$$\overline{\boldsymbol{N}}_{\boldsymbol{\gamma}}^\star(\boldsymbol{s}) = \underset{\boldsymbol{a} \in \mathcal{A}}{\mathbb{N}} \left\{\boldsymbol{c_N}(\boldsymbol{s}, \boldsymbol{a}) + \delta \mathbb{E}_{Pr}\left[\overline{\boldsymbol{N}}_{\boldsymbol{\gamma}}^\star(\boldsymbol{s}')\right]\right\}, \tag{34}$$

$$\overline{\boldsymbol{D}}_{\boldsymbol{\gamma}}^\star(\boldsymbol{s}) = \underset{\boldsymbol{a} \in \mathcal{A}}{\mathbb{N}} \left\{\boldsymbol{c_D}(\boldsymbol{s}, \boldsymbol{a}) + \delta \mathbb{E}_{Pr}\left[\overline{\boldsymbol{D}}_{\boldsymbol{\gamma}}^\star(\boldsymbol{s}')\right]\right\}, \tag{35}$$

where specifically, $\overline{\boldsymbol{N}}_{\boldsymbol{\gamma}}^\star(\boldsymbol{s}) = \left[\overline{N}_{\gamma_m}^\star(\boldsymbol{s})\right]_{m \in \mathcal{M}}$ and $\overline{\boldsymbol{D}}_{\boldsymbol{\gamma}}^\star(\boldsymbol{s}) = \left[\overline{D}_{\gamma_m}^\star(\boldsymbol{s})\right]_{m \in \mathcal{M}}$. Then we have $\boldsymbol{V}_{\boldsymbol{\gamma}}^\star(\boldsymbol{s}) = \overline{\boldsymbol{N}}_{\boldsymbol{\gamma}}^\star(\boldsymbol{s}) - \boldsymbol{\gamma}\overline{\boldsymbol{D}}_{\boldsymbol{\gamma}}^\star(\boldsymbol{s})$.

For each sub-game $G_{\boldsymbol{\gamma}}$, we perform the fractional Nash Q-Learning algorithm to obtain the optimal value function $\boldsymbol{V}_{\boldsymbol{\gamma}}^\star(\boldsymbol{s})$. Each episode terminates when the sub-game achieves Nash equilibrium.

2) Outer loop: The outer loop implements the iteration of fraction sub-games following Dinkelbach method [23]. After achieving the NE of sub-game $G_{\boldsymbol{\gamma}}$, we update the quotient coefficient in line 9 of Algorithm 2 as :

$$\gamma_m = \underset{\boldsymbol{s}_0 \sim \mu_0}{\mathbb{E}}\left[\frac{\overline{N}_{\gamma_m}(\boldsymbol{s}_0)}{\overline{D}_{\gamma_m}(\boldsymbol{s}_0)}\right], \forall m \in \mathcal{M}. \tag{36}$$

We repeat this process until $\boldsymbol{\gamma}$ converges. The equivalence between game G and fractional sub-games $\{G_{\boldsymbol{\gamma}}\}$ and the convergence of $\boldsymbol{\gamma}$ is discussed in the following subsection.

D. Convergence Analysis

We are ready to present the convergence results of Algorithm 2for the game G. This facilitates us to adapt the convergence proof in [23] to our framework.

We first examine the existence of an equivalent condition of reaching NE between the Markov game G and the fractional sub-game $G_{\boldsymbol{\gamma}}$ with the following lemma:

Lemma 3. *There exists $\boldsymbol{\gamma} \succ \mathbf{0}$, such that $\underset{\boldsymbol{s}_0 \sim \mu_0}{\mathbb{E}}\left[\boldsymbol{V}_{\boldsymbol{\gamma}}^\star(\boldsymbol{s}_0)\right] = \mathbf{0}$ at the NE of sub-game $G_{\boldsymbol{\gamma}}$.*

Lemma 3 is mainly proven using the Brouwer fixed point theorem. The detailed proof can be found in Appendix C. We then analyze the equivalence for reaching NE between the game G and the fractional sub-game $G_{\boldsymbol{\gamma}}$ as follows.

Lemma 4. *Markov game G attains Nash equilibrium strategies $\boldsymbol{\pi}^\star$ if and only if sub-game $G_{\boldsymbol{\gamma}^\star}$ achieves the Nash equilibrium and $\underset{\boldsymbol{s}_0 \sim \mu_0}{\mathbb{E}}\left[\boldsymbol{V}_{\boldsymbol{\gamma}^\star}^\star(\boldsymbol{s}_0)\right] = \mathbf{0}$.*

The proof Lemma 4 established upon the result of Lemma 3. See Appendix D for proof. We define two conditions when sub-game $G_{\boldsymbol{\gamma}}$ attains an NE as follows.

Definition 4 (Global optimum)**.** *A strategy profile $(\boldsymbol{\pi}_m^\star, \boldsymbol{\pi}_{-m}^\star)$ is a global optimal point if, for all agents $m \in \mathcal{M}$, the following inequality holds:*

$$V_{\gamma_m}(\boldsymbol{s}, \boldsymbol{\pi}_m^\star, \boldsymbol{\pi}_{-m}^\star) \leq V_{\gamma_m}(\boldsymbol{s}, \boldsymbol{\pi}_m, \boldsymbol{\pi}_{-m}), \forall \boldsymbol{\pi}_m, \boldsymbol{\pi}_{-m}. \tag{37}$$

Definition 5 (Saddle Point)**.** *A strategy profile $(\boldsymbol{\pi}_m^\star, \boldsymbol{\pi}_{-m}^\star)$ is a saddle point if, for all agents $m \in \mathcal{M}$, the following inequalities holds:*

$$V_{\gamma_m}(\boldsymbol{s}, \boldsymbol{\pi}_m^\star, \boldsymbol{\pi}_{-m}^\star) \leq V_{\gamma_m}(\boldsymbol{s}, \boldsymbol{\pi}_m, \boldsymbol{\pi}_{-m}^\star), \quad \forall \boldsymbol{\pi}_m, \tag{38}$$

$$V_{\gamma_m}(\boldsymbol{s}, \boldsymbol{\pi}_m^\star, \boldsymbol{\pi}_{-m}^\star) \geq V_{\gamma_m}(\boldsymbol{s}, \boldsymbol{\pi}_m^\star, \boldsymbol{\pi}_{-m}), \quad \forall \boldsymbol{\pi}_{-m}. \tag{39}$$

Assumption 1. *For each sub-game in training, the Nash equilibrium $(\boldsymbol{\pi}_m^\star, \boldsymbol{\pi}_{-m}^\star)$ of sub-game $G_{\boldsymbol{\gamma}}$ is recognized either as global optimum in Definition 4 or a saddle point in Definition 5.*

This assumption is adopted in theoretical frameworks analyzing MARL [59], and is widely applied in MARL algorithms, such as Nash Q-learning [24], Mean-field MARL [60] and Friend-or-Foe Q-learning [61].

Choose $\overline{\gamma} = \max_{\mathbf{s},\mathbf{a}} \left\{ \frac{c_{N,m}(\mathbf{s},\mathbf{a})}{c_{D,m}(\mathbf{s},\mathbf{a})} \right\}$. Then for any $\boldsymbol{s}_0$, we have $\frac{N_{\gamma_m}(\boldsymbol{s}_0)}{D_{\gamma_m}(\boldsymbol{s}_0)} \leq \overline{\gamma}$. Define a compact and convex set $\Gamma = [0, \overline{\gamma}]^M$ and mapping $\mathbb{T} : \Gamma \to \Gamma$ of $\boldsymbol{\gamma}$ in Algorithm 2 as:

$$\mathbb{T}\boldsymbol{\gamma} = \left[\mathop{\mathbb{E}}_{\boldsymbol{s}_0 \sim \mu_0} \left[\frac{\overline{N}_{\gamma_1}(\boldsymbol{s}_0)}{\overline{D}_{\gamma_1}(\boldsymbol{s}_0)} \right], \ldots, \mathop{\mathbb{E}}_{\boldsymbol{s}_0 \sim \mu_0} \left[\frac{\overline{N}_{\gamma_M}(\boldsymbol{s}_0)}{\overline{D}_{\gamma_M}(\boldsymbol{s}_0)} \right] \right]^T. \quad (40)$$

We present the definition of contraction mapping and the contraction mapping of $\mathbb{T}$ as follows.

Definition 6. *(Contraction Mapping) Let $(\mathcal{X}, d)$ be a metric space and $\mathbb{L} : \mathcal{X} \to \mathcal{X}$ be a mapping. The mapping $\mathbb{L}$ is a contraction mapping if there exists $\rho \in [0, 1)$ such that:*

$$d(\mathbb{L}x, \mathbb{L}y) \leq \rho \cdot d(x, y), \forall x, y \in \mathcal{X}. \quad (41)$$

Theorem 2. *(Contraction Mapping of $\mathbb{T}$)*

Under Assumption 1, mapping $\mathbb{T}$ is a contraction mapping. That is, there exists $\rho \in [0, 1)$ such that $\|\mathbb{T}\boldsymbol{\gamma}^\star - \mathbb{T}\boldsymbol{\gamma}\| \preceq \rho \|\boldsymbol{\gamma}^\star - \boldsymbol{\gamma}\|$ in Algorithm 2.

Please refer to Appendix E for detailed proof. Thus, Algorithm 2 converges to NE of game G.

VI. Asynchronous Fractional MADRL Algorithm

In this section, we introduce A. F. MADRL, an asynchronous fractional MADRL algorithm. This algorithm achieves NE for the SMG Problem (7) with hybrid action space, as shown in Fig. 2.

Building on the fractional MARL framework proposed in Section V, we first introduce a fractional cost module of $\boldsymbol{\gamma}$. This module approximates NE when optimizing the fractional AoI objective in multi-agent scenario. However, when considering the scheduling problem of MEC formulated as SMG, synchronized decision-making and training become inefficient due to asynchronous task completions. To address the challenge of asynchronous decision-making, we introduce an asynchronous trajectory collection mechanism. Additionally, we propose the corresponding hybrid strategy and value networks to apply the mechanism for hybrid action spaces of updating and offloading actions.

A. Fractional Cost Module

As in the proposed fractional MARL framework in Section V, we consider a set of episodes $i \in [E]$ and introduce a quotient coefficient γ_i for episode i. We define $\boldsymbol{a}_i^H = [\boldsymbol{a}_{m,i}^H]_{m=1}^M$, where $\boldsymbol{a}_{m,i}^H \triangleq [(\boldsymbol{a}_m^{\mathrm{U}}, \boldsymbol{a}_m^{\mathrm{O}})]_{k=1}^K$ as the set of updating and offloading strategies of mobile device $m \in \mathcal{M}$ in episode i, where superscript 'H' refers to 'history'.

At each task k, we determine a fractional cost and send it for training. This process corresponds to the sub-game of the proposed fractional RL framework. Based on (28), we define the cost for all $i \in [E], m \in \mathcal{M}$, and $k \in \mathcal{K}$ as:

$$\begin{aligned} c_{m,i}^k(\boldsymbol{a}_m^H, \boldsymbol{a}_{-m}^H) =& A(Y_{m,k}^i, Z_{m,k+1}^i, Y_{m,k+1}^i) \\ & - \gamma_m \cdot (Y_{m,k}^i + Z_{m,k+1}^i), \end{aligned} \quad (42)$$

where for episode i, $Y_{m,k}^i$ denotes the duration of task k , $Z_{m,k+1}^i$ is the waiting time before generating task $k+1$, and $A(Y_{m,k}^i, Z_{m,k+1}^i, Y_{m,k+1}^i)$ represents the trapezoid area in (3). Note that $Y_{m,k}$ is a function of $\boldsymbol{a}_m^{\mathrm{U}}$, and $Z_{m,k+1}$ is a function of $(\boldsymbol{a}_m^H, \boldsymbol{a}_{-m}^H)$. The fractional cost module tracks $(\boldsymbol{a}_m^H, \boldsymbol{a}_{-m}^H)$, or equivalently $Y_{m,k}$ and $Z_{m,k}$ for all $k = 0, 1, ..., K$ throughout the training process.

Finally, at the end of each episode m, the fractional cost module updates $\gamma_{m,i+1}$ by:

$$\gamma_{m,i+1} = \frac{\sum_{k=0}^{K} \delta^k A_m(Y_{m,k}, Z_{m,k+1}, Y_{m,k+1})}{\sum_{k=0}^{K} \delta^k (Y_{m,k} + Z_{m,k+1})}. \quad (43)$$

B. Asynchronous Trajectory Collection Mechanism

To train MADRL algorithms, we collect trajectories from agents, including global states, local observations, actions, and costs. Traditional MADRL algorithms such as MADDPG [20] and MAPPO require synchronous joint information from all agents at each time step, making them unsuitable for asynchronous decision-makings. VarlenMARL [45], an asynchronous MADRL algorithm, addresses this by allowing variable-length trajectories. However, it still struggles to fully utilize agent interactions in asynchronous environments.

Our method introduces a novel asynchronous trajectory collection mechanism. It collects agent trajectories based on a global clock T and aggregates historical decision-making at local task level asynchronously. This approach incorporates global states and other agents' actions, better leveraging agent interactions and asynchronous collaboration. We compare our asynchronous mechanism with traditional MARL and VarlenMARL with 2 agents as follows.

Traditional MARL algorithms gather joint data of all agents at the each time step. The joint trajectory collected is

$$[(s_1, \boldsymbol{a}_{1,1}, \boldsymbol{a}_{2,1}), (s_2, \boldsymbol{a}_{1,2}, \boldsymbol{a}_{2,2}), (s_3, \boldsymbol{a}_{1,3}, \boldsymbol{a}_{2,3}), \cdots].$$

VarlenMARL [45] allows agents to collect trajectories asynchronously. It merges an agent's data with the latest padded data from other agents. Let $\boldsymbol{s}_m^0, \boldsymbol{a}_m^0$ be the initial trajectory of agent m. Fig. 3(a) shows the trajectories of Agent 1 and Agent 2 as:

$$\begin{aligned} &[(\boldsymbol{s}_{1,1}, \boldsymbol{a}_{1,1}, (\boldsymbol{s}_{2,0}, \boldsymbol{a}_{2,0})), (\boldsymbol{s}_{1,2}, \boldsymbol{a}_{1,2}, (\boldsymbol{s}_{2,1}, \boldsymbol{a}_{2,1})), \\ &(\boldsymbol{s}_{1,3}, \boldsymbol{a}_{1,3}, (\boldsymbol{s}_{2,1}, \boldsymbol{a}_{2,1})) \cdots], [(\boldsymbol{s}_{2,1}, \boldsymbol{a}_{2,1}, (\boldsymbol{s}_{1,1}, \boldsymbol{a}_{1,1})), \\ &(\boldsymbol{s}_{2,2}, \boldsymbol{a}_{2,2}, (\boldsymbol{s}_{1,3}, \boldsymbol{a}_{1,3})), (\boldsymbol{s}_{2,3}, \boldsymbol{a}_{2,3}, (\boldsymbol{s}_{1,3}, \boldsymbol{a}_{1,3})), \cdots]. \end{aligned}$$

However, training becomes problematic when agents' task timelines are significantly unsynchronized. For example, Agent 2's information at global task 7 is overlooked and not used for padding.

Our proposed asynchronous trajectory collection mechanism as shown in Fig. 3(b), enables agents to collect trajectories asynchronously in execution time order. We define time-aggregating information $\{H_T\}$, updated by $H_{T+1} = TA[(\boldsymbol{s}_l, \boldsymbol{a}_l), H_T]$, where TA is time-aggregating function and

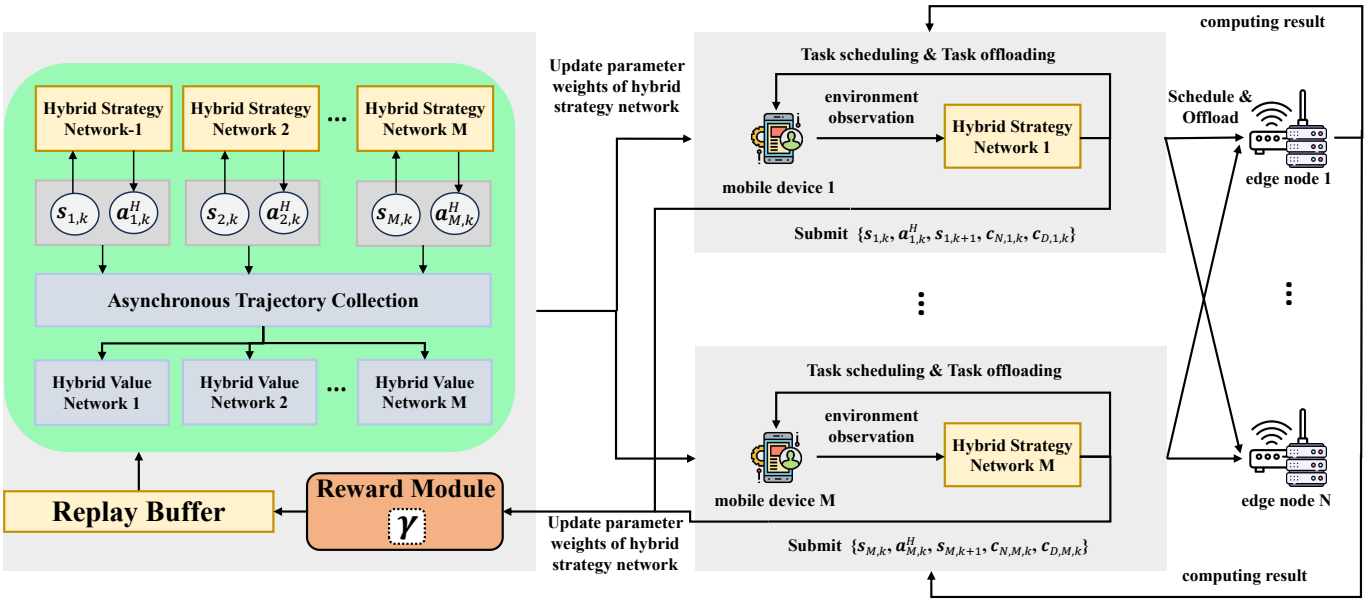

Fig. 2. Illustration on the proposed asynchronous fractional MADRL framework with fractional cost module, asynchronous trajectory collection mechanism, and hybrid strategy and value networks with R-D3QN and R-PPO.

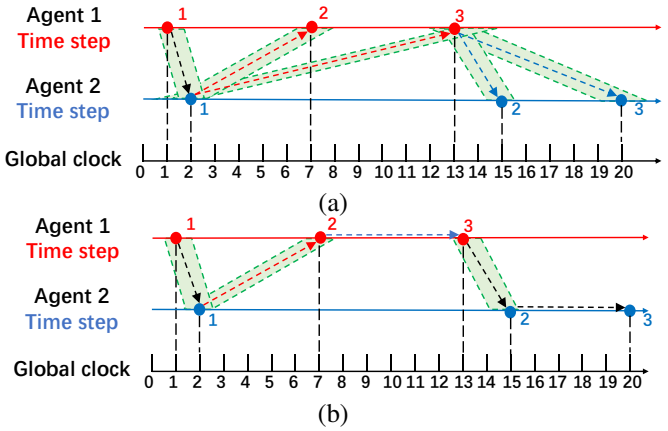

Fig. 3. Comparison of trajectory collection mechanisms under VarlenMARL, and our proposed RNN-PPO. (a) In VarlenMARL, agent collects its trajectory as well as the latest information from other agents. (b) In RNN-PPO, agent collects its trajectory with the time-aggregating information from history decision events.

$(\boldsymbol{s}_l, \boldsymbol{a}_l)$ is the latest state-action tuple. Additionally, agent m collects the H_T at global clock T. This mechanism enables more accurate state and Q value evaluations using global states, actions, and aggregated information from all agents' previous actions. The collected trajectory as shown in Fig. 3(b) is:

$$[(\boldsymbol{s}_{1,1}, \boldsymbol{a}_{1,1}, H_1), (\boldsymbol{s}_{2,1}, \boldsymbol{a}_{2,1}, H_2), (\boldsymbol{s}_{1,2}, \boldsymbol{a}_{1,2}, H_3), (\boldsymbol{s}_{1,3}, \boldsymbol{a}_{1,3}, H_4), (\boldsymbol{s}_{2,2}, \boldsymbol{a}_{2,2}, H_5), (\boldsymbol{s}_{2,3}, \boldsymbol{a}_{2,3}, H_6), \cdots].$$

This mechanism allows agents to collect trajectories asynchronously and utilize time-aggregated information from past events in practical task order during execution and training.

C. Hybrid Strategy Network

Our algorithm trains hybrid strategy and value networks for each mobile device in the fractional framework, enabling asynchronous decision-making of hybrid actions.[2]

The asynchronous trajectory collection mechanism synthesizes time-aggregating data. It utilizing state-action pairs from other agents and historical events to improve agent interactions. We implement this mechanism with RNN, applying it to both D3QN (for discrete action spaces) and PPO (for continuous action spaces). Then, we form the RNN-D3QN (R-D3QN) and RNN-PPO (R-PPO) with corresponding strategy and value networks as detailed in Appendix F. These hybrid networks address both the task offloading and updating processes.

VII. Performance Evaluation

We evaluate our fractional multi-agent framework with experiments involving 20 mobile devices. Our experimental setup primarily follows the settings outlined in [14, Table I], with additional details provided in Appendix G. We compare our proposed algorithms and baseline algorithms as follows.

- *Non-Fractional MADRL (denoted by Non-F. MADRL)*: This benchmark let each mobile devices learn hybrid DRL algorithms individually, without fractional scheme. It exploits the D3QN networks to generate discrete action for offloading decisions and PPO networks with continuous action for updating decisions. In comparison to our proposed fractional framework, this benchmark is non-fractional and is lack of the asynchronous trajectory collection mechanism. It approximates the ratio-of-expectation average AoI by an expectation-of-ratio expression: minimize$_{\boldsymbol{\pi}_m}$ $\mathbb{E}\left[\frac{A(Y_{m,k}, Z_{m,k+1}, Y_{m,k+1})}{Y_{m,k}+Z_{m,k+1}} \middle| \boldsymbol{\pi}_m\right]$. This approximation to tackle the fractional challenge tends to cause large accuracy loss.

[2]We centrally train the hybrid networks in a trusted third-party.

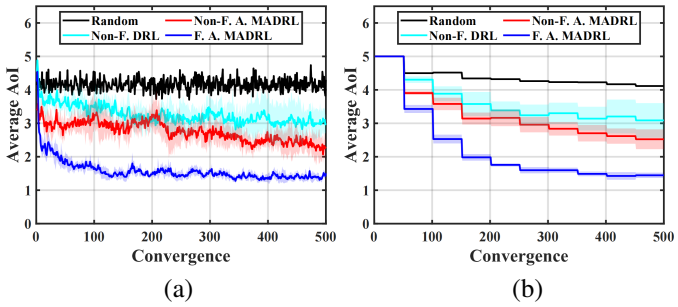

Fig. 4. Convergence of (a) average AoI and (b) the average value of quotient coefficients γ across devices, where γ is updated every 50 episodes.

- *Asynchronous Non-Fractional MADRL (denoted by A. Non-F. MADRL)*: This benchmark incorporates the asynchronous trajectory collection mechanism into the Non-F. MADRL algorithm to demonstrate its effectiveness. While it employs the same asynchronous trajectory collection mechanism as our proposed A. F. MADRL algorithm, it lacks the fractional framework.
- *A. F. MADRL*: The proposed A. F. MADRL algorithm incorporates two key elements. First, it uses a fractional scheme to approximate the NE. Second, it employs a trajectory collection mechanism, which aggregates information from both historical records and other agents.
- *Random*: This method randomly schedules updating and offloading decisions within the action spaces.
- *H-MAPPO*: Multi-agent proximal policy optimization [22] with hybrid action spaces.
- *VarlenMARL*: VarLenMARL [45] implements independent time steps with variable lengths for each agent. It utilizes a synchronized delay-tolerant mechanism to enhance performance. This approach is discussed in Section II and VI.

Our experiments first evaluate the convergence of our proposed algorithms. We then compare their performance against baselines. Our experiments systematically evaluate several factors: edge capacity, drop coefficient, task density, mobile capacity, processing variance, and number of agents.

Convergence: Fig. 4 shows the convergence of Non-F. DRL and proposed A. Non-F. MADRL and A. F. MADRL algorithms. We not only evaluate the convergence of target metric of our proposed algorithms but also compare the average fractional coefficient γ, which are supposed to converge simultaneously. In Fig. 4(a), A. Non-F. MADRL and A. F. MADRL algorithms converge after about 300 episodes. Regarding to the converged average AoI, A. F. MADRL outperforms Non-F. DRL by 53.7%. Specifically, the performance gap between A. Non-F. MADRL and Non-F. DRL demonstrates the necessity of our proposed fractional framework. Additionally, the performance difference between A. F. MADRL and A. Non-F. MADRL highlights the significance of our proposed asynchronous trajectory collection mechanism.

Edge Capacity: In Fig. 5(a), we evaluate different processing capacities of edge servers. Compared to Non-F. MADRL, Non-A. F. MADRL reduces the average AoI about 28.1% on average with the asynchronous trajectory collection scheme. The proposed A. F. MADRL algorithm consistently achieves smaller average AoI compared to other benchmarks that don't consider fractional AoI and asynchronous settings. It reduces the average AoI by up to 36.0% compared to H-MAPPO at 55 GHz. This demonstrates that better design for asynchronous setting can achieves superior performance when more edge capacity is available to exploit.

Drop Coefficient: Fig. 5(b) illustrates the results of different drop coefficients, which are the ratios of drop time $\bar{Y}$ to the task processing duration. While the average AoI of random scheduling decreases as the drop coefficient increases, other RL techniques show no clear trend. This suggests that the updating policy may serve as a dropping mechanism. With different drop coefficients, our proposed A. F. MADRL algorithm archives about 32.9% less average AoI compared against H-MAPPO on average.

Task Density: Fig. 5(c) shows the AoI performance under varying task densities. These densities affect overall task loads and expected processing duration at mobile devices and edge servers. Our A. F. MADRL algorithm outperforms all other benchmarks. At 15 Gigacycles per Mbits, A. F. MADRL reduces the average AoI by up to 41.3% and 63.5% compared to H-MAPPO and Non-F. MADRL, respectively. Non-A. F. MADRL outperforms Non-F. MADRL by 17.5% on average, which demonstrates the effectiveness of our asynchronous trajectory collection mechanism.

Mobile Capacity: Fig. 5(d), presents results for different mobile device capacities. Our A. F. MADRL algorithm reduces average AoI by 39.1% on average compared to Non-F. DRL algorithm. Performance gaps narrow at high mobile device capacities. This occurs because devices with high capacities process most tasks locally. Consequently, the effectiveness of task scheduling diminishes.

Processing Variance: Fig. 5(e) demonstrates the performance of algorithms under different variances of processing time. In this particular experiment, processing times are modeled using a lognormal distribution. Algorithms with asynchronous trajectory collection such as VarlenMARL and A. F. MADRL show significant performance advantages at relatively higher variances (e.g., 1.1, 1.3), This indicates that the asynchronous trajectory collection mechanism works well when decision steps of mobile devices vary dramatically over time. Additionally, A. F. MADRL algorithm outperforms VarlenMARL in most cases.

Number of Mobile Devices: Fig. 5(f) shows the performance with varying numbers of mobile devices and fixed edge servers. The proposed A. F. MADRL algorithm outperforms H-MAPPO by up to 52.6% with 5 mobile devices. Additionally, the performance gap between A. F. MADRL and A. Non-F. MADRL narrows when the number of mobile devices is either very small or very high. This trend indicates that both algorithms, which incorporate the proposed asynchronous trajectory collection mechanism, can achieve superior performance when the number of mobile devices is small. In such scenarios, tasks are mainly offloaded to edge nodes. Conversely, when the number of mobile devices is large, tasks are primarily processed locally. In this case, the impact of the scheduling policy is limited.

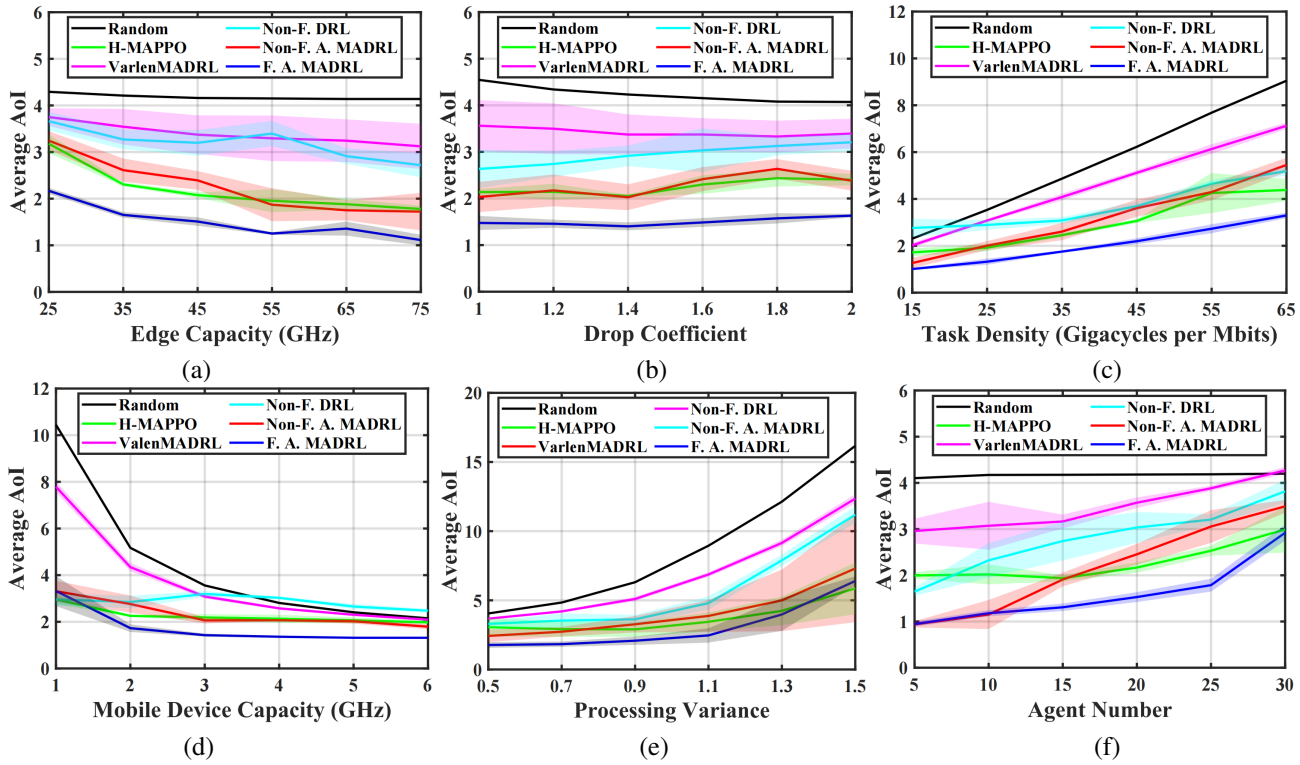

Fig. 5. Performance under different (a) processing capacities of edges, (b) drop coefficients, (c) task densities, (d) processing capacities of mobile devices, (e) processing variances, (f) number of agents.

VIII. Conclusion

In this paper, we proposed three schemes for computational task scheduling (including offloading and updating) age-minimal MEC in a semi-Markov game. First, we introduce a fractional RL framework for single-agent scenario with fractional objectives. Second, we develop a fractional MARL framework for fractional scheme in multi-agent scenarios. We demonstrate that this framework theoretically converges to Nash equilibrium. Third, we present an asynchronous trajectory collection mechanism to address asynchronous multi-agent problems in SMG. Evaluation results show significant performance improvements in average AoI for both the fractional framework and asynchronous trajectory collection mechanism. In future works, it's worth concerning the energy consumption and security satisfaction in MEC systems, which may also be formulated as fractional objectives.

References

[1] L. Jin, M. Tang, M. Zhang, and H. Wang, "Fractional deep reinforcement learning for age-minimal mobile edge computing," in *Proceedings of the AAAI Conference on Artificial Intelligence*, vol. 38, no. 11, 2024, pp. 12 947–12 955.

[2] D. Katare, D. Perino, J. Nurmi, M. Warnier, M. Janssen, and A. Y. Ding, "A survey on approximate edge ai for energy efficient autonomous driving services," *IEEE Communications Surveys & Tutorials*, 2023.

[3] Z. Xu, W. Jiang, J. Xu, Y. Deng, S. Cheng, and J. Zhao, "A power-grid-mapping edge computing structure for digital distributed distribution networks," *IEEE Transactions on Smart Grid*, 2023.

[4] J. Jin, K. Yu, J. Kua, N. Zhang, Z. Pang, and Q.-L. Han, "Cloud-fog automation: Vision, enabling technologies, and future research directions," *IEEE Transactions on Industrial Informatics*, vol. 20, no. 2, pp. 1039–1054, 2023.

[5] P. Porambage *et al.*, "Survey on multi-access edge computing for Internet of things realization," *IEEE Commun. Surveys & Tuts.*, vol. 20, no. 4, pp. 2961–2991, Jun. 2018.

[6] Y. Mao, C. You, J. Zhang, K. Huang, and K. B. Letaief, "A survey on mobile edge computing: The communication perspective," *IEEE Commun. Surveys & Tuts.*, vol. 19, no. 4, pp. 2322–2358, Aug. 2017.

[7] Q. Abbas, S. A. Hassan, H. K. Qureshi, K. Dev, and H. Jung, "A comprehensive survey on age of information in massive iot networks," *Computer Communications*, vol. 197, pp. 199–213, 2023.

[8] C. Xu *et al.*, "AoI-centric task scheduling for autonomous driving systems," in *Proc. IEEE INFOCOM*, May 2022.

[9] J. Cao, X. Zhu, S. Sun, Z. Wei, Y. Jiang, J. Wang, and V. K. Lau, "Toward industrial metaverse: Age of information, latency and reliability of short-packet transmission in 6g," *IEEE Wireless Communications*, vol. 30, no. 2, pp. 40–47, 2023.

[10] C. Zhu, G. Pastor, Y. Xiao, and A. Ylajaaski, "Vehicular fog computing for video crowdsourcing: Applications, feasibility, and challenges," *IEEE Communications Magazine*, vol. 56, no. 10, pp. 58–63, 2018.

[11] X. Xu, K. Liu, K. Xiao, L. Feng, Z. Wu, and S. Guo, "Vehicular fog computing enabled real-time collision warning via trajectory calibration," *Mobile Networks and Applications*, vol. 25, pp. 2482–2494, 2020.

[12] S. Kaul, R. Yates, and M. Gruteser, "Real-time status: How often should one update?" in *Proc. IEEE INFOCOM*, 2012, pp. 2731–2735.

[13] S. Wang, Y. Guo, N. Zhang, P. Yang, A. Zhou, and X. Shen, "Delay-aware microservice coordination in mobile edge computing: A reinforcement learning approach," *IEEE Trans. Mobile Comput.*, vol. 20, no. 3, pp. 939 – 951, Mar. 2021.

[14] M. Tang and V. W. Wong, "Deep reinforcement learning for task offloading in mobile edge computing systems," *IEEE Trans. Mobile Comput.*, vol. 21, no. 6, pp. 1985–1997, 2022.

[15] J. Hao, T. Yang, H. Tang, C. Bai, J. Liu, Z. Meng, P. Liu, and Z. Wang, "Exploration in deep reinforcement learning: From single-agent to multiagent domain," *IEEE Transactions on Neural Networks and Learning Systems*, 2023.

[16] H. Ma, P. Huang, Z. Zhou, X. Zhang, and X. Chen, "Greenedge: Joint green energy scheduling and dynamic task offloading in multi-tier edge computing systems," *IEEE Transactions on Vehicular Technology*, vol. 71, no. 4, pp. 4322–4335, Apr. 2022.

[17] N. Zhao, Z. Ye, Y. Pei, Y.-C. Liang, and D. Niyato, "Multi-agent deep

reinforcement learning for task offloading in UAV-assisted mobile edge computing," *IEEE Trans. Wireless Commun.*, 2022.

[18] X. He, S. Wang, X. Wang, S. Xu, and J. Ren, "Age-based scheduling for monitoring and control applications in mobile edge computing systems," in *Proc. IEEE INFOCOM*, May 2022.

[19] X. Chen *et al.*, "Information freshness-aware task offloading in air-ground integrated edge computing systems," *IEEE J. Sel. Areas Commun.*, vol. 40, no. 1, pp. 243–258, Jan. 2022.

[20] R. Lowe, Y. I. Wu, A. Tamar, J. Harb, O. Pieter Abbeel, and I. Mordatch, "Multi-agent actor-critic for mixed cooperative-competitive environments," *Advances in neural information processing systems*, vol. 30, 2017.

[21] T. Rashid, M. Samvelyan, C. S. De Witt, G. Farquhar, J. Foerster, and S. Whiteson, "Monotonic value function factorisation for deep multi-agent reinforcement learning," *The Journal of Machine Learning Research*, vol. 21, no. 1, pp. 7234–7284, 2020.

[22] C. Yu, A. Velu, E. Vinitsky, J. Gao, Y. Wang, A. Bayen, and Y. Wu, "The surprising effectiveness of ppo in cooperative multi-agent games," *Advances in Neural Information Processing Systems*, vol. 35, pp. 24 611–24 624, 2022.

[23] W. Dinkelbach, "On nonlinear fractional programming," *Management science*, vol. 13, no. 7, pp. 492–498, May 1967.

[24] J. Hu and M. P. Wellman, "Nash q-learning for general-sum stochastic games," *Journal of machine learning research*, vol. 4, no. Nov, pp. 1039–1069, 2003.

[25] Y. Chen, J. Zhao, J. Hu, S. Wan, and J. Huang, "Distributed task offloading and resource purchasing in noma-enabled mobile edge computing: Hierarchical game theoretical approaches," *ACM Trans. Embed. Comput. Syst.*, vol. 23, no. 1, jan 2024.

[26] H. Taka, F. He, and E. Oki, "Service placement and user assignment in multi-access edge computing with base-station failure," in *Proc. IEEE/ACM IWQoS*, Jun. 2022.

[27] S. Liu, C. Zheng, Y. Huang, and T. Q. S. Quek, "Distributed reinforcement learning for privacy-preserving dynamic edge caching," *IEEE J. Sel. Areas Commun.*, vol. 40, no. 3, pp. 749–760, Mar. 2022.

[28] X. Wang, J. Ye, and J. C. Lui, "Decentralized task offloading in edge computing: A multi-user multi-armed bandit approach," in *Proc. IEEE Conference on Computer Communications (INFOCOM)*, May 2022.

[29] L. Huang, S. Bi, and Y.-J. A. Zhang, "Deep reinforcement learning for online computation offloading in wireless powered mobile-edge computing networks," *IEEE Trans. Mobile Comput.*, vol. 19, no. 11, pp. 2581 – 2593, Nov. 2020.

[30] S. Tuli *et al.*, "Dynamic scheduling for stochastic edge-cloud computing environments using A3C learning and residual recurrent neural networks," *IEEE Trans. Mobile Comput.*, vol. 21, no. 3, Mar. 2022.

[31] T. Liu *et al.*, "Deep reinforcement learning based approach for online service placement and computation resource allocation in edge computing," *IEEE Trans. Mobile Comput.*, 2022.

[32] Q. Li, X. Ma, A. Zhou, X. Luo, F. Yang, and S. Wang, "User-oriented edge node grouping in mobile edge computing," *IEEE Transactions on Mobile Computing*, 2021.

[33] Z. Feng, M. Huang, Y. Wu, D. Wu, J. Cao, I. Korovin, S. Gorbachev, and N. Gorbacheva, "Approximating nash equilibrium for anti-uav jamming markov game using a novel event-triggered multi-agent reinforcement learning," *Neural Networks*, vol. 161, pp. 330–342, 2023. [Online]. Available: https://www.sciencedirect.com/science/article/pii/S0893608022005226

[34] F. Yuan, S. Tang, and D. Liu, "Aoi-based transmission scheduling for cyber-physical systems over fading channel against eavesdropping," *IEEE Internet of Things Journal*, 2023.

[35] X. Fu, Q. Pan, and X. Huang, "Aoi-energy-aware collaborative data collection in uav-enabled wireless powered sensor networks," *IEEE Sensors Journal*, 2023.

[36] R. D. Yates, Y. Sun, D. R. Brown, S. K. Kaul, E. Modiano, and S. Ulukus, "Age of information: An introduction and survey," *IEEE J. Sel. Areas Commun.*, vol. 39, no. 5, pp. 1183–1210, 2021.

[37] F. Chiariotti, O. Vikhrova, B. Soret, and P. Popovski, "Peak age of information distribution for edge computing with wireless links," *IEEE Trans. Commun.*, vol. 69, no. 5, pp. 3176–3191, 2021.

[38] E. T. Ceran, D. Gündüz, and A. György, "A reinforcement learning approach to age of information in multi-user networks with HARQ," *IEEE J. Sel. Areas Commun.*, vol. 39, no. 5, pp. 1412–1426, 2021.

[39] M. Akbari *et al.*, "Age of information aware vnf scheduling in industrial iot using deep reinforcement learning," *IEEE J. Sel. Areas Commun.*, vol. 39, no. 8, pp. 2487–2500, 2021.

[40] X. Chen *et al.*, "Age of information aware radio resource management in vehicular networks: A proactive deep reinforcement learning perspective," *IEEE Trans. Wireless Commun.*, vol. 19, no. 4, 2020.

[41] F. Wu, H. Zhang, J. Wu, Z. Han, H. V. Poor, and L. Song, "UAV-to-device underlay communications: Age of information minimization by multi-agent deep reinforcement learning," *IEEE Transactions on Communications*, vol. 69, no. 7, pp. 4461–4475, 2021.

[42] Z. Ren and B. Krogh, "Markov decision processes with fractional costs," *IEEE Transactions on Automatic Control*, vol. 50, no. 5, pp. 646–650, 2005.

[43] T. Tanaka, "A partially observable discrete time markov decision process with a fractional discounted reward," *Journal of Information and Optimization Sciences*, vol. 38, no. 1, pp. 21–37, 2017.

[44] W. Suttle, K. Zhang, Z. Yang, J. Liu, and D. Kraemer, "Reinforcement learning for cost-aware markov decision processes," in *Proceedings of the 38th International Conference on Machine Learning*, ser. Proceedings of Machine Learning Research, M. Meila and T. Zhang, Eds., vol. 139. PMLR, 18–24 Jul 2021, pp. 9989–9999. [Online]. Available: https://proceedings.mlr.press/v139/suttle21a.html

[45] Y. Chen, H. Wu, Y. Liang, and G. Lai, "Varlenmarl: A framework of variable-length time-step multi-agent reinforcement learning for cooperative charging in sensor networks," in *2021 18th Annual IEEE International Conference on Sensing, Communication, and Networking (SECON)*. IEEE, 2021, pp. 1–9.

[46] Y. Liang, H. Wu, and H. Wang, "Asm-ppo: Asynchronous and scalable multi-agent ppo for cooperative charging," in *Proceedings of the 21st International Conference on Autonomous Agents and Multiagent Systems*, 2022, pp. 798–806.

[47] Y. Sun, E. Uysal-Biyikoglu, R. D. Yates, C. E. Koksal, and N. B. Shroff, "Update or wait: How to keep your data fresh," *IEEE Trans. Inform. Theory*, vol. 63, no. 11, pp. 7492–7508, 2017.

[48] A. Arafa, R. D. Yates, and H. V. Poor, "Timely cloud computing: Preemption and waiting," in *Proc. Allerton*, 2019.

[49] Y. Sun and B. Cyr, "Sampling for data freshness optimization: Non-linear age functions," *Journal of Communications and Networks*, vol. 21, no. 3, pp. 204–219, 2019.

[50] A. Arafa, J. Yang, S. Ulukus, and H. V. Poor, "Age-minimal transmission for energy harvesting sensors with finite batteries: Online policies," *IEEE Transactions on Information Theory*, vol. 66, no. 1, pp. 534–556, 2019.

[51] M. Zhang, A. Arafa, J. Huang, and H. V. Poor, "Pricing fresh data," *IEEE J. Sel. Areas Commun.*, vol. 39, no. 5, pp. 1211–1225, 2021.

[52] Z. Tang, Z. Sun, N. Yang, and X. Zhou, "Age of information analysis of multi-user mobile edge computing systems," in *Proc. IEEE GLOBECOM*, Dec. 2021.

[53] J. Zhu and J. Gong, "Online scheduling of transmission and processing for aoi minimization with edge computing," in *Proc. IEEE INFOCOM WKSHPS*, May 2022.

[54] J. Li, Y. Zhou, and H. Chen, "Age of information for multicast transmission with fixed and random deadlines in IoT systems," *IEEE Internet of Things Journal*, vol. 7, no. 9, pp. 8178–8191, Sep. 2020.

[55] M. Ghavamzadeh, H. Kappen, M. Azar, and R. Munos, "Speedy q-learning," in *Proc. Neural Info. Process. Syst. (NIPS)*, vol. 24, 2011.

[56] D. Adelman and A. J. Mersereau, "Relaxations of Weakly Coupled Stochastic Dynamic Programs," *Operations Research*, Jan. 2008, publisher: INFORMS. [Online]. Available: https://pubsonline.informs.org/doi/abs/10.1287/opre.1070.0445

[57] A. M. Fink, "Equilibrium in a stochastic n-person game," *Journal of science of the hiroshima university, series ai (mathematics)*, vol. 28, no. 1, pp. 89–93, 1964.

[58] P. Casgrain, B. Ning, and S. Jaimungal, "Deep q-learning for nash equilibria: Nash-dqn," *Applied Mathematical Finance*, vol. 29, no. 1, pp. 62–78, 2022.

[59] J. Hu, M. P. Wellman *et al.*, "Multiagent reinforcement learning: theoretical framework and an algorithm." in *ICML*, vol. 98, 1998, pp. 242–250.

[60] Y. Yang, R. Luo, M. Li, M. Zhou, W. Zhang, and J. Wang, "Mean field multi-agent reinforcement learning," in *International conference on machine learning*. PMLR, 2018, pp. 5571–5580.

[61] M. L. Littman *et al.*, "Friend-or-foe q-learning in general-sum games," in *ICML*, vol. 1, no. 2001, 2001, pp. 322–328.

[62] V. Mnih *et al.*, "Human-level control through deep reinforcement learning," *Nature*, vol. 518, no. 7540, pp. 529–533, Feb. 2015.

[63] H. Van Hasselt, A. Guez, and D. Silver, "Deep reinforcement learning with double q-learning," in *Proceedings of the AAAI conference on artificial intelligence*, vol. 30, no. 1, 2016.

[64] Z. Wang, T. Schaul, M. Hessel, H. Hasselt, M. Lanctot, and N. Freitas, "Dueling network architectures for deep reinforcement learning," in *International conference on machine learning*. PMLR, 2016, pp. 1995–2003.
[65] M. Hausknecht and P. Stone, "Deep recurrent q-learning for partially observable mdps," in *2015 aaai fall symposium series*, 2015.

APPENDIX A
TIME COMPLEXITY OF INNER LOOP IN FQL ALGORITHM

Proposition 1. *Proposed FQL Algorithm satisfies the stopping condition $\epsilon_i < -\alpha Q_i(\boldsymbol{s}_0, \boldsymbol{a}_i)$ for some $\alpha \in (0,1)$, then after*

$$T_i = \left\lceil \frac{11.66 \log(2|\mathcal{Z}|/(E\zeta))}{\alpha^2} \right\rceil \tag{44}$$

steps of SQL in [55], the uniform approximation error $\|Q^*_{\gamma_i} - Q_i\| \leq \epsilon_i$ holds for all $i \in [E]$, with a probability of $1-\zeta$ for any $\zeta \in (0,1)$.

Proof Sketch: The main proof of Proposition 1 is based on [55]. Specifically, we can prove that the required T_i is proportional to Q_i^2/ϵ_i^2, and hence corresponding to a constant upper bound.

Proposition 1 shows that the total steps needed T_i does not increase in i, even though the stopping condition $\epsilon_i < -\alpha Q_i(\boldsymbol{s}_0, \boldsymbol{a}_i)$ is getting more restrictive as i increases.

APPENDIX B
PROOF OF THEOREM 1

Define

$$\boldsymbol{a}^*(\gamma) \triangleq \arg\max_{a \in \mathcal{A}} \left(N_\gamma(\boldsymbol{s}_0, \boldsymbol{a}) - \gamma D_\gamma(\boldsymbol{s}_0, \boldsymbol{a})\right), \tag{45a}$$

$$Q(\gamma) \triangleq \max_{\boldsymbol{a} \in \mathcal{A}} \left(N_\gamma(\boldsymbol{s}_0, \boldsymbol{a}) - \gamma D_\gamma(\boldsymbol{s}_0, \boldsymbol{a})\right), \tag{45b}$$

$$N(\gamma) = N_\gamma(s_0, \boldsymbol{a}^*(\gamma)) \quad \text{and} \quad D(\gamma) = D_\gamma(s_0, \boldsymbol{a}^*(\gamma)), \tag{45c}$$

$$F(\gamma) = \frac{N(\gamma)}{D(\gamma)}, \tag{45d}$$

$$\boldsymbol{a}_i \triangleq \arg\max_{\boldsymbol{a} \in \mathcal{A}} \left(N_k(\boldsymbol{s}_0, \boldsymbol{a}) - \gamma D_k(\boldsymbol{s}_0, \boldsymbol{a})\right), \tag{45e}$$

for all $\gamma \geq 0$. In the remaining part of this proof, we use $Q_i = Q_i(\boldsymbol{s}_0, \boldsymbol{a}_i)$, $N_i = N_i(\boldsymbol{s}_0, \boldsymbol{a}_i)$, and $D_i = D_i(\boldsymbol{s}_0, \boldsymbol{a}_i)$ for presentation simplicity. Note that

$$\begin{aligned} & \frac{N(\gamma')}{D(\gamma')} - \frac{N_i}{D_i} \\ \overset{(a)}{\geq} \; & \frac{N(\gamma')}{D(\gamma')} - \frac{N(\gamma')}{D_i} - \gamma \left[\frac{D(\gamma')}{D_i} - \frac{D(\gamma')}{D(\gamma)}\right] - \frac{\epsilon_i}{D_i} \\ = \; & [-Q(\gamma') + (\gamma_i - \gamma')D(\gamma')] \left(\frac{1}{D_i} - \frac{1}{D(\gamma')}\right) - \frac{\epsilon_i}{D_i}, \end{aligned} \tag{46}$$

where (a) is from the suboptimality of N_i. Sequences $\{\gamma_i\}$, $\{Q_i\}$, and $\{D_i\}$ generated by FQL Algorithm satisfy

$$\gamma_i - \gamma^* \geq \gamma_i - N_i/D_i = -Q_i/D_i > \epsilon_i/\alpha D_i, \tag{47}$$

for all i such that $Q_i < 0$. In addition, from the fact that $N_i - \gamma_i D_i \leq N(\gamma^*) - \gamma_i D(\gamma^*)$ and $N(\gamma^*) - \gamma^* D(\gamma^*) \leq N_i - \gamma^* D_i$ for all $i \in [E]$, it follows that $(\gamma_i - \gamma^*)(D(\gamma^*) - D_i) \leq 0$, $\forall i \in [E]$, and hence $\gamma_i \geq \gamma^*$ if and only if $D_i \geq D(\gamma^*)$. It follows from (46) that, for all i,

$$\begin{aligned} \gamma_{i+1} - \gamma^* = F_i - \gamma^* \leq \; & (\gamma_i - \gamma^*) \left(1 - \frac{D(\gamma^*)}{D_i}\right) + \frac{\epsilon_i}{D_i} \\ \overset{(b)}{<} \; & (\gamma_i - \gamma^*) \left(1 + \alpha - \frac{D(\gamma^*)}{D_i}\right). \end{aligned}$$

Note that (b) is inducted from (47). Specifically, if $\gamma_i < \gamma^*$, then $\gamma_{i+1} < \gamma^*$. Therefore, we have that, if $Q_i < 0$ then $Q_{i+1} < 0$, and hence that $\epsilon_i \leq -\alpha Q_i$ for all $i \in [E]$. There exists $\alpha \in (0,1)$, such that $(\gamma_{i+1} - \gamma^*)/(\gamma_i - \gamma^*) \in (0,1)$ for all large enough i, which implies that $\{\gamma_i\}$ converges linearly to γ^*.

APPENDIX C
PROOF OF LEMMA 3

The Bellman equation form of V_{γ_m} of mobile device m is given by:

$$\begin{aligned} V_{\gamma_m}(\boldsymbol{s}, \boldsymbol{\pi}) = & \mathbb{E}_{\boldsymbol{\pi}} \left\{ c_{N_m}(\boldsymbol{s}, \boldsymbol{a}) - \gamma_m c_{D_m}(\boldsymbol{s}, \boldsymbol{a}) \right. \\ & \left. + \mathbb{E}_{Pr}[\delta V_{\gamma_m}(\boldsymbol{s}', \boldsymbol{\pi})] \right]\}. \end{aligned} \tag{48}$$

Let $\mathcal{B}(\mathcal{S})$ denote the Banach space of bounded real-valued functions on $\mathcal{S}$ with the supremum norm. Let $\mathbb{W}_{\boldsymbol{\pi}} : \mathcal{B}(\mathcal{S}) \to \mathcal{B}(\mathcal{S})$ be the mapping:

$$\begin{aligned} \mathbb{W}_{\boldsymbol{\pi}} V_{\gamma_m}(\boldsymbol{s}, \boldsymbol{\pi}) = & \min_{\boldsymbol{\pi}_m} \mathbb{E}_{\boldsymbol{\pi}} \left\{ [c_{N_m}(\boldsymbol{s}, \boldsymbol{a}) - \gamma_m c_{D_m}(\boldsymbol{s}, \boldsymbol{a}) \right. \\ & \left. + \delta \mathbb{E}_{Pr}[V_{\gamma_m}(\boldsymbol{s}', \boldsymbol{\pi})]] \right\}. \end{aligned} \tag{49}$$

From [57], we have the following conclusion:

Theorem C.3. *(Contraction Mapping of $\mathbb{W}_{\boldsymbol{\pi}}$) For any fixed γ_m and $\boldsymbol{s} \in \mathcal{S}$, $\mathbb{W}_{\boldsymbol{\pi}}$ is a contraction mapping of $\mathbb{R}$.*

By Theorem C.3, the sequence $V^0_{\gamma_m} = 0$, $V^{k+1}_{\gamma_m} = \mathbb{W}_{\boldsymbol{\pi}} V^k_{\gamma_m}$ converges to the optimal cost $V^\star_{\gamma_m}(\boldsymbol{s})$:

$$\begin{aligned} V^\star_{\gamma_m}(\boldsymbol{s}) = & \min_{\boldsymbol{\pi}_m} \mathbb{E}_{\boldsymbol{\pi}} \left\{ c_{N_m}(\boldsymbol{s}, \boldsymbol{a}) - \gamma_m c_{D_m}(\boldsymbol{s}, \boldsymbol{a}) \right. \\ & \left. + \delta \mathbb{E}_{Pr}[V^\star_{\gamma_m}(\boldsymbol{s}')] \right\}. \end{aligned} \tag{50}$$

Lemma C.5. *$V^\star_{\gamma_m}$ is continuous with respect to γ_m.*

Proof. Define function f as

$$\begin{aligned} f(\gamma_m, \boldsymbol{\pi}, \boldsymbol{s}) = & \mathbb{E}_{\boldsymbol{\pi}} \left\{ c_{N_m}(\boldsymbol{s}, \boldsymbol{a}) - \gamma_m c_{D_m}(\boldsymbol{s}, \boldsymbol{a}) \right. \\ & \left. + \delta \mathbb{E}_{Pr}[V^*_{\gamma_m}(\boldsymbol{s}')] \right\}. \end{aligned} \tag{51}$$

From (50), we have

$$V^\star_{\gamma_m}(\boldsymbol{s}) = \min_{\boldsymbol{\pi}_m} f(\gamma_m, \boldsymbol{\pi}, \boldsymbol{s}). \tag{52}$$

Since $c_{N_m}(\boldsymbol{s}, \boldsymbol{a})$, $c_{D_m}(\boldsymbol{s}, \boldsymbol{a})$ is continuous with respect to $\boldsymbol{\pi}$, we have $f(\gamma_m, \boldsymbol{\pi}, \boldsymbol{s})$ is continuous with respect to $\boldsymbol{\pi}$ and γ_m. Thus, as the set of $\boldsymbol{\pi}$ is a compact set, by Berge's maximum theorem, we have $V^\star_{\gamma_m}(\boldsymbol{s})$ is continuous with respect to γ_m. ∎

Since $c_{N_m}(\boldsymbol{s}, \boldsymbol{a})$, $c_{D_m}(\boldsymbol{s}, \boldsymbol{a})$ are continuous with respect to γ_m, from (33), we have Nash operator $\underset{\boldsymbol{a} \in \mathcal{A}}{\boldsymbol{\mathcal{N}}}$ is continuous with respect to γ_m. From (34), we have $N_{\gamma_m}(\boldsymbol{s}), D_{\gamma_m}(\boldsymbol{s})$ are continuous with respect to γ_m.

Theorem C.4. *(Existence of Fixed Point) There exists a fixed point $\boldsymbol{\gamma}^\star$ for mapping $\mathbb{T}$, such that $\mathbb{T}\boldsymbol{\gamma}^\star = \boldsymbol{\gamma}^\star$.*

Proof. Since $D_{\gamma_m}(\boldsymbol{s}_0) \neq 0$, mapping $\mathbb{T}$ is continuous on $\boldsymbol{\gamma}$. By Brouwer fixed point theorem, there exists a fixed point $\boldsymbol{\gamma}^\star \in \Gamma$ for continuous mapping $\mathbb{T}$. ■

Therefore, there exists $\boldsymbol{\gamma}^\star$, such that $\mathbb{T}\boldsymbol{\gamma}^\star = \boldsymbol{\gamma}^\star$. Then we have $\mathop{\mathbb{E}}_{\boldsymbol{s}_0\sim\mu_0}\left[\frac{\overline{\boldsymbol{N}}_{\boldsymbol{\gamma}^\star}(\boldsymbol{s}_0)}{\overline{\boldsymbol{D}}_{\boldsymbol{\gamma}^\star}(\boldsymbol{s}_0)}\right] = \boldsymbol{\gamma}^\star$. Thus, we have $\mathop{\mathbb{E}}_{\boldsymbol{s}_0\sim\mu_0}\left[\boldsymbol{V}^\star_{\boldsymbol{\gamma}^\star}(\boldsymbol{s}_0)\right] = \mathop{\mathbb{E}}_{\boldsymbol{s}_0\sim\mu_0}\left[\overline{\boldsymbol{N}}^\star_{\boldsymbol{\gamma}^\star}(\boldsymbol{s}_0)\right] - \boldsymbol{\gamma}^\star \odot \mathop{\mathbb{E}}_{\boldsymbol{s}_0\sim\mu_0}\left[\overline{\boldsymbol{D}}^\star_{\boldsymbol{\gamma}^\star}(\boldsymbol{s}_0) = 0\right]$.

APPENDIX D
PROOF OF LEMMA 4

Define

$$\overline{N}(\boldsymbol{\pi}^\star_m, \boldsymbol{\pi}^\star_{-m}) = \mathbb{E}_{\boldsymbol{s}_0\sim\mu_0}[\overline{N}^\star_{\gamma^\star_m}(\boldsymbol{s}_0)], \tag{53a}$$
$$\overline{D}(\boldsymbol{\pi}^\star_m, \boldsymbol{\pi}^\star_{-m}) = \mathbb{E}_{\boldsymbol{s}_0\sim\mu_0}[\overline{N}^\star_{\gamma^\star_m}(\boldsymbol{s}_0)], \tag{53b}$$

where $(\boldsymbol{\pi}^\star_1, \ldots, \boldsymbol{\pi}^\star_M)$ is the NE of game G defined in Section V with respect to $\boldsymbol{\gamma}^\star$. We prove that game G reaches NE if and only if the sub-game $G_{\boldsymbol{\gamma}}$ reaches NE as follows.

(a) Assume $(\boldsymbol{\pi}^\star_1, \ldots, \boldsymbol{\pi}^\star_M)$ be the Nash equilibrium of game G. We have for each agent m,

$$\gamma^\star_m = \frac{\overline{N}(\boldsymbol{\pi}^\star_m, \boldsymbol{\pi}^\star_{-m})}{\overline{D}(\boldsymbol{\pi}^\star_m, \boldsymbol{\pi}^\star_{-m})} \geq \frac{\overline{N}(\boldsymbol{\pi}_m, \boldsymbol{\pi}^\star_{-m})}{\overline{D}(\boldsymbol{\pi}_m, \boldsymbol{\pi}^\star_{-m})} \tag{54}$$

Hence,

$$\overline{N}(\boldsymbol{\pi}^\star_m, \boldsymbol{\pi}^\star_{-m}) - \gamma^\star_m \overline{D}(\boldsymbol{\pi}^\star_m, \boldsymbol{\pi}^\star_{-m}) = 0, \tag{55}$$

and

$$\begin{aligned}&\overline{N}(\boldsymbol{\pi}^\star_m, \boldsymbol{\pi}^\star_{-m}) - \gamma^\star_m \overline{D}(\boldsymbol{\pi}^\star_m, \boldsymbol{\pi}^\star_{-m})\\ &\geq \overline{N}(\boldsymbol{\pi}_m, \boldsymbol{\pi}^\star_{-m}) - \gamma^\star_m \overline{D}(\boldsymbol{\pi}_m, \boldsymbol{\pi}^\star_{-m})\end{aligned} \tag{56}$$

Thus, $\boldsymbol{\pi}^\star_1, \ldots, \boldsymbol{\pi}^\star_M$ is also the Nash equilibrium of the sub-game $G^{\boldsymbol{\gamma}}$.

(b) Conversely, assume $(\boldsymbol{\pi}^\star_1, \ldots, \boldsymbol{\pi}^\star_M)$ be the Nash equilibrium of the sub-game $G_{\boldsymbol{\gamma}}$ and for each mobile device $m \in \mathcal{M}$ $\overline{N}(\boldsymbol{\pi}^\star_m, \boldsymbol{\pi}^\star_{-m}) - \gamma^\star_m \overline{D}(\boldsymbol{\pi}^\star_m, \boldsymbol{\pi}^\star_{-m}) = 0$. We have

$$\gamma^\star_m = \frac{\overline{N}(\boldsymbol{\pi}^\star_m, \boldsymbol{\pi}^\star_{-m})}{\overline{D}(\boldsymbol{\pi}^\star_m, \boldsymbol{\pi}^\star_{-m})}, \tag{57}$$

which means game G converges on sub-game G_i with the Γ_i iterations and from Definition 1, for each agent m we have

$$\begin{aligned}&\overline{N}(\boldsymbol{\pi}^\star_m, \boldsymbol{\pi}^\star_{-m}) - \gamma^\star_m \overline{D}(\boldsymbol{\pi}^\star_m, \boldsymbol{\pi}^\star_{-m})\\ &\geq \overline{N}(\boldsymbol{\pi}_m, \boldsymbol{\pi}^\star_{-m}) - \gamma^\star_m \overline{D}(\boldsymbol{\pi}_m, \boldsymbol{\pi}^\star_{-m})\end{aligned} \tag{58}$$

Hence,

$$\frac{\overline{N}(\boldsymbol{\pi}^\star_m, \boldsymbol{\pi}^\star_{-m})}{\overline{D}(\boldsymbol{\pi}^\star_m, \boldsymbol{\pi}^\star_{-m})} \geq \frac{\overline{N}(\boldsymbol{\pi}_m, \boldsymbol{\pi}^\star_{-m})}{\overline{D}(\boldsymbol{\pi}_m, \boldsymbol{\pi}^\star_{-m})} \tag{59}$$

APPENDIX E
PROOF OF THEOREM 2

We denote the ith sub-game as $G_{\boldsymbol{\gamma}_i}$ and the corresponding NE as $\boldsymbol{\pi}_i$ for $i \in \mathcal{N}$.

We prove the convergence of game G with our framework of iterative sub-games under Assumption 1 for each mobile device m as follows.

Case 1: When $(\boldsymbol{\pi}_{1,i}, \ldots, \boldsymbol{\pi}_{M,i})$ and $(\boldsymbol{\pi}^\star_1, \ldots, \boldsymbol{\pi}^\star_M)$ satisfy Condition A in Assumption 1 for their sub-games respectively, which means they are both global optimal points. From Condition A of Assumption 1, for any NE $\boldsymbol{\pi}^\star$ of sub-games we have

$$\begin{aligned}&\overline{N}(\boldsymbol{\pi}_m, \boldsymbol{\pi}_{-m}) - \gamma^\star_m \overline{D}(\boldsymbol{\pi}_m, \boldsymbol{\pi}_{-m})\\ &\leq \overline{N}(\boldsymbol{\pi}^\star_m, \boldsymbol{\pi}^\star_{-m}) - \gamma^\star_m \overline{D}(\boldsymbol{\pi}^\star_m, \boldsymbol{\pi}^\star_{-m}) = 0, \forall m.\end{aligned} \tag{60}$$

Hence, $\frac{\overline{N}(\boldsymbol{\pi}_{m,i}, \boldsymbol{\pi}_{-m,i})}{\overline{D}(\boldsymbol{\pi}_{m,i}, \boldsymbol{\pi}_{-m,i})} \leq \frac{\overline{N}(\boldsymbol{\pi}^\star_m, \boldsymbol{\pi}^\star_{-m})}{\overline{D}(\boldsymbol{\pi}^\star_m, \boldsymbol{\pi}^\star_{-m})}$ and $\gamma^i < \gamma^\star$. Also from Condition A of Assumption 1 with assumption error we have,

$$\overline{N}(\boldsymbol{\pi}_{m,i}, \boldsymbol{\pi}_{-m,i}) - \gamma_{m,i} \overline{D}(\boldsymbol{\pi}_{m,i}, \boldsymbol{\pi}_{-m,i}) \tag{61}$$
$$\geq \overline{N}(\boldsymbol{\pi}^\star_m, \boldsymbol{\pi}^\star_{-m}) - \gamma_{m,i} \overline{D}(\boldsymbol{\pi}^\star_m, \boldsymbol{\pi}^\star_{-m}), \forall m. \tag{62}$$

Thus, for each mobile device m, we have

$$\begin{aligned}&|\gamma^*_m - \gamma_{m,i+1}|\\ =&\frac{\overline{N}(\boldsymbol{\pi}^\star_m, \boldsymbol{\pi}^\star_{-m})}{\overline{D}(\boldsymbol{\pi}^\star_m, \boldsymbol{\pi}^\star_{-m})} - \frac{\overline{N}(\boldsymbol{\pi}_{m,i}, \boldsymbol{\pi}_{-m,i})}{\overline{D}(\boldsymbol{\pi}_{m,i}, \boldsymbol{\pi}_{-m,i})}\\ \leq&\gamma^\star_m - \gamma_{m,i} - \frac{\overline{N}(\boldsymbol{\pi}^\star_m, \boldsymbol{\pi}^\star_{-m}) - \gamma_{m,i}\overline{D}(\boldsymbol{\pi}^\star_m, \boldsymbol{\pi}^\star_{-m})}{\overline{D}(\boldsymbol{\pi}_{m,i}, \boldsymbol{\pi}_{-m,i})}\\ \leq&(\gamma^\star_m - \gamma_{m,i})\left[1 - \frac{\overline{D}(\boldsymbol{\pi}^\star_m, \boldsymbol{\pi}^\star_{-m})}{\overline{D}(\boldsymbol{\pi}_{m,i}, \boldsymbol{\pi}_{-m,i})}\right].\end{aligned} \tag{63}$$

Hence, we have $\frac{|\gamma^*_m - \gamma_{m,i+1}|}{|\gamma^\star_m - \gamma_{m,i}|} \in (0, 1)$.

Case 2: When $(\boldsymbol{\pi}_{1,i}, \ldots, \boldsymbol{\pi}_{M,i})$ and $(\boldsymbol{\pi}^\star_1, \ldots, \boldsymbol{\pi}^\star_n)$ satisfy Condition B in Assumption 1, which means they are saddle points.

From Definition 1 with approximation error we have,

$$\overline{N}(\boldsymbol{\pi}_{m,i}, \boldsymbol{\pi}_{-m,i}) - \gamma_{m,i} \overline{D}(\boldsymbol{\pi}_{m,i}, \boldsymbol{\pi}_{-m,i}) \tag{64}$$
$$\geq \overline{N}(\boldsymbol{\pi}^\star_m, \boldsymbol{\pi}_{-m,i}) - \gamma_{m,i} \overline{D}(\boldsymbol{\pi}^\star_m, \boldsymbol{\pi}_{-m,i}) \tag{65}$$

From Condition B of Assumption 1 we have,

$$\overline{N}(\boldsymbol{\pi}^\star_m, \boldsymbol{\pi}^\star_{-m}) - \gamma^\star_m \overline{D}(\boldsymbol{\pi}^\star_m, \boldsymbol{\pi}^\star_{-m}) \tag{66}$$
$$\leq \overline{N}(\boldsymbol{\pi}^\star_m, \boldsymbol{\pi}_{-m,i}) - \gamma^\star_m \overline{D}(\boldsymbol{\pi}^\star_m, \boldsymbol{\pi}_{-m,i}) \tag{67}$$

Case 2.1: Suppose $\gamma^\star_m \geq \gamma_{m,i+1}$ and $\gamma^\star_m \geq \gamma_{m,i}$, we have

$$\begin{aligned}&|\gamma^*_m - \gamma_{m,i+1}|\\ \leq&\gamma^\star_m - \gamma_{m,i} - \frac{\overline{N}(\boldsymbol{\pi}^\star_m, \boldsymbol{\pi}_{-m,i}) - \gamma_{m,i}\overline{D}(\boldsymbol{\pi}^\star_m, \boldsymbol{\pi}_{-m,i})}{\overline{D}(\boldsymbol{\pi}_{m,i}, \boldsymbol{\pi}_{-m,i})}\\ \leq&(\gamma^\star_m - \gamma_{m,i})\left[1 - \frac{\overline{D}(\boldsymbol{\pi}^\star_m, \boldsymbol{\pi}_{-m,i})}{\overline{D}(\boldsymbol{\pi}_{m,i}, \boldsymbol{\pi}_{-m,i})}\right]\end{aligned} \tag{68}$$

Hence, we have $\frac{|\gamma_m^*-\gamma_{m,i+1}|}{|\gamma_m^\star-\gamma_{m,i}|}\in(0,1)$.

Case 2.2: Suppose $\gamma_m^\star\leq\gamma_{m,i+1}$ and $\gamma_m^\star\leq\gamma_{m,i}$, we have

$$|\gamma_m^*-\gamma_{m,i+1}|\leq(\gamma_{m,i}-\gamma_m^\star)\left[1-\frac{\overline{D}(\boldsymbol{\pi}_{m,i},\boldsymbol{\pi}_{-m}^\star)}{\overline{D}(\boldsymbol{\pi}_{m,i},\boldsymbol{\pi}_{-m,i})}\right]. \tag{69}$$

Then, $\frac{|\gamma_m^*-\gamma_{m,i+1}|}{|\gamma_m^\star-\gamma_{m,i}|}\in(0,1)$.

Case 2.3: When there exist $i,j\in\mathcal{N}(i<j)$, $\gamma_{m,i}\leq\gamma_m^\star$, $\gamma_{m,i+1}\geq\gamma_m^\star$, $\gamma_m^j\geq\gamma_m^\star$ and $\gamma_{m,j+1}\leq\gamma_m^\star$, $\gamma_{m,i+1}\geq\gamma_m^\star$.

$$\begin{aligned}
&|\gamma_m^*-\gamma_{m,j+1}|\\
\leq&(\gamma_m^\star-\gamma_m^j)\left[1-\frac{\overline{D}(\boldsymbol{\pi}_m^\star,\boldsymbol{\pi}_{-m,j})}{\overline{D}(\boldsymbol{\pi}_{m,j},\boldsymbol{\pi}_{-m,j})}\right]\\
\leq&(\gamma_m^\star-\gamma_m^{j-1})\left[1-\frac{\overline{D}(\boldsymbol{\pi}_m^\star,\boldsymbol{\pi}_{-m,j-1})}{\overline{D}(\boldsymbol{\pi}_{m,j-1},\boldsymbol{\pi}_{-m,j-1})}\right]\\
&\left[1-\frac{\overline{D}(\boldsymbol{\pi}_m^\star,\boldsymbol{\pi}_{-m,j})}{\overline{D}(\boldsymbol{\pi}_{m,j},\boldsymbol{\pi}_{-m,j})}\right]\\
\leq&(\gamma_m^\star-\gamma_{m,i})\left[1-\frac{\overline{D}(\boldsymbol{\pi}_m^\star,\boldsymbol{\pi}_{-m,i})}{\overline{D}(\boldsymbol{\pi}_m^i,\boldsymbol{\pi}_{-m}^i)}\right]\cdots\\
&\left[1-\frac{\overline{D}(\boldsymbol{\pi}_m^\star,\boldsymbol{\pi}_{-m,j})}{\overline{D}(\boldsymbol{\pi}_{m,j},\boldsymbol{\pi}_{-m,j})}\right]
\end{aligned} \tag{70}$$

Since $\gamma_m^\star-\gamma_{m,i}\geq0$, we have $\frac{|\gamma_m^*-\gamma_{m,j}|}{|\gamma_m^\star-\gamma_{m,i}|}\in(0,1)$ holds.

Case 2.4: When there exist $i,j\in\mathcal{N}(i<j)$, $\gamma_{m,i}\geq\gamma_m^\star$, $\gamma_{m,i+1}\leq\gamma_m^\star$, $\gamma_m^j\leq\gamma_m^\star$ and $\gamma_{m,j+1}\geq\gamma_m^\star$, $\gamma_{m,i+1}\leq\gamma_m^\star$.

$$\begin{aligned}
&|\gamma_m^*-\gamma_{m,j+1}|\\
\leq&(\gamma_{m,j}-\gamma_m^\star)\left[1-\frac{\overline{D}(\boldsymbol{\pi}_{m,j},\boldsymbol{\pi}_{-m}^\star)}{\overline{D}(\boldsymbol{\pi}_{m,j},\boldsymbol{\pi}_{-m,j})}\right]\\
\leq&(\gamma_{m,i}-\gamma_m^\star)\left[1-\frac{\overline{D}(\boldsymbol{\pi}_m^i,\boldsymbol{\pi}_{-m}^\star)}{\overline{D}(\boldsymbol{\pi}_m^i,\boldsymbol{\pi}_{-m}^i)}\right]\cdots\\
&\left[1-\frac{\overline{D}(\boldsymbol{\pi}_{m,j},\boldsymbol{\pi}_{-m}^\star)}{\overline{D}(\boldsymbol{\pi}_{m,j},\boldsymbol{\pi}_{-m,j})}\right]
\end{aligned} \tag{71}$$

Since $\gamma_{m,i}-\gamma_m^\star\geq0$, we have $\frac{|\gamma_m^*-\gamma_{m,j}|}{|\gamma_m^\star-\gamma_{m,i}|}\in(0,1)$ holds.

Thus, there exists $\rho\in[0,1)$ such that $\|\mathbb{T}\boldsymbol{\gamma}^\star-\mathbb{T}\boldsymbol{\gamma}\|\preceq\rho\|\boldsymbol{\gamma}^\star-\boldsymbol{\gamma}\|$ in Algorithm 2.

APPENDIX F
ASYNCHRONOUS FRACTIONAL MULTI-AGENT DRL NETWORKS

As shown in Fig. 6, for each mobile device, our algorithm contains R-D3QN and R-PPO networks for discrete and continuous action space as well as interactions between agents and history information.

A. R-D3QN Module

D3QN is a modified version of deep Q-learning [62] equipped with double DQN technique with target Q to overcome overestimation [63] and dueling DQN technique which separately estimates value function and advantage function [64]. And our R-D3QN structure is inspired by DRQN [65]

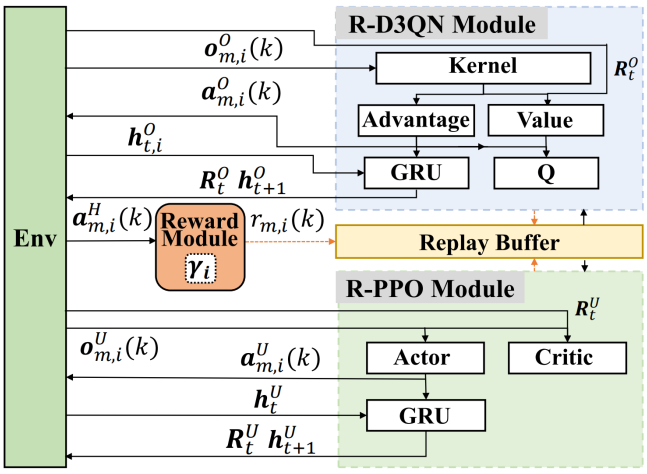

Fig. 6. Illustration on the proposed fractional multi-agent DRL framework of D3QN and PPO module with RNN networks including reward module with proposed fractional scheme and GRU module with asynchronous trajectory collection mechanism.

which allows networks to retain context and memory from history events and environment states. The key idea is to learn a mapping from states in state space S^O to the Q-value of actions in action space A^O. When the policy is learned and updated to the mobile device, it can selective offloading actions with the maximum Q-value to maximize the expected long-term reward. Apart from traditional deep Q-learning, it has a target Q-function network to compute the expected long-term reward of based on the optimal action chosen with the traditional Q-function network to solve the overestimation problem. What's more, both the Q-function networks contain the advantage layer and value layer, which are used to estimate the value of the state and the relative advantage of the action. What's more, we take advantage of a GRU module to provide history information of other agents' decisions and environment states.

B. R-PPO Module

R-PPO mainly includes two networks: policy network and value network. Policy network is responsible for producing actions based on networks. It outputs mean and standard deviation vectors for continuous action and probability distribution for discrete network. The value network computes the advantage values and estimates the expected return of the current state. Similar to R-D3QN network, it has an additional GRU module to memory the state-action pairs from history and other agents to enhance the information contained by the state based on which the value network estimates the state value.